Fe3O4 imbuing carboxymethyl cellulose/dextran sulfate nanocomposite hydrogel beads: an effective adsorbent for methylene blue dye pollutant

Fe_3O_4 imbuing carboxymethyl cellulose/dextran sulfate nanocomposite hydrogel beads: an effective adsorbent for methylene blue dye pollutant

Tayeb Benhalima[a,b], Hafida Ferfera-Harrar[a], Nabanita Saha[c], and Petr Saha[c]

[a]*Materials Polymer Laboratory, Macromolecular Chemistry Department, University of Sciences and Technology Houari Boumediene, USTHB, Algiers, Algeria*

[b]*Unité de Recherche en Analyses et Developpement Technologiques en Environnement-Centre de Recherche Scientifique et Technique en Analyses Physico-Chimiques (UR-ADTE-CRAPC), Tipaza, Algeria*

[c]*University Institute, Tomas Bata University in Zlin, Zlin, Czech Republic*

CONTACT: *Tayeb Benhalima @ tayeb4647@yahoo.fr; Hafida Ferfera-Harrar @ harrarhafida@yahoo.fr Materials Polymer Laboratory, Macromolecular Chemistry Department, University of Sciences and Technology Houari Boumediene, USTHB, B.P. 32 El-Alia, Algiers, 16111, Algeria*

GRAPHICAL ABSTRACT

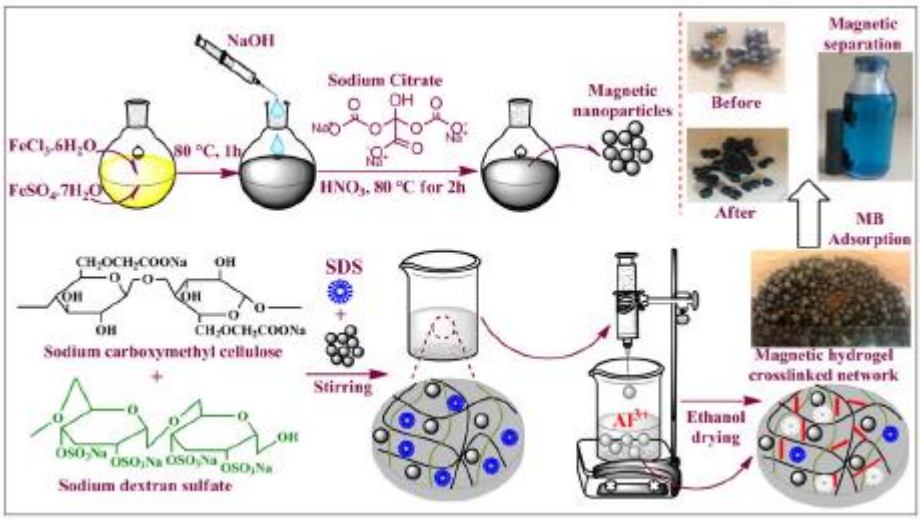

ABSTRACT

In this study, initially synthesized magnetic nanoparticles modified with citrate ions (MNPs/m-MNPs) were entrapped in aluminum-carboxymethyl cellulose/dextran sulfate beads to form hybrid nanocomposites (m-MNPs-C/D0.5) using a simple two-pot method. Sodium dodecyl sulfate surfactant was employed to develop a porous interconnected structure. The synergistic effect of the hybrid nanocomposites was studied for the parametric adsorption of methylene blue dye pollutant. The swelling ability of hybrid hydrogels was also studied for different solution pH. The results clearly

indicated that equilibrium was reached faster at about 3 h for the m-MNPs-loaded magnetic beads (m-MNPs-C/D0.5), whereas at 6 h for the MNPs-loaded beads (MNPs0.4-C/D0.5) and the unloaded simple ones (MNPs0-C/D0.5). Experimental data modeling of adsorption kinetics and isotherms as well as thermodynamic study showed a good correlation with pseudo-second order kinetic and Langmuir models while the adsorption process on magnetic beads was exothermic. The maximum adsorption capacity for MNPs0-C/D0.5 and the optimized m-MNPs0.3-C/D0.5 hydrogel were 380 and 529 mg g^{-1}, respectively. Furthermore, all hydrogels were perfectly regenerated and then reused for five adsorption-desorption cycles without apparent loss of stability that confirms their consideration as alternative and effective adsorbents for wastewater treatment. The manufactured beads were characterized by scanning electron microscopy/energy dispersive X-Ray, dynamic light scattering, X-ray diffraction, thermogravimetric analysis, vibrating sample magnetometer and fourier-transform infrared spectroscopy.

KEYWORDS: Magnetic nanocomposites hydrogel beads, carboxymethyl cellulose, dextran sulfate, dye removal, regeneration, adsorption-desorption cycles

1. Introduction

Over the past few years, climate warming, global population growth and insufficient water resources have made the remediation of polluted waters an obvious and urgent neces-sity.[1] Such pollution is mainly generated by the discharge of some dangerous chemical compounds (phenolic compounds, heavy metals, dyes, insecticides etc.) by several industries: chemical, textile, tannery, food processing, pharmaceutical and so on.[2,3] The impact of these industrial effluents on the fauna and flora is extremely harmful.[4] Awareness raising of the public and socio-economic actors, accompanied by strict regulations on effluent disposal, would help prevent this drift and thus save what can still be saved. Among organic or inorganic pollutants, dyes are considered as the most harmful even though they are most often found at trace levels, due to their highly toxic and carcinogenic nature and their non-degradable and persistent nature. [5,6] It cannot be metabolized by the body and accumulates in living organisms, causing various diseases and disorders such as cancer, damage to functional organs and the nervous system and in extreme cases death. In front of this critical situation and the collective awareness, considerable efforts have been spent over the decades to satisfy health and environmental concerns related to water contamination. Research in this field is growing. The objective is to develop the most robust, economically feasible, easy, and environmentally friendly treatment processes. In this context, many water treatment methods are used for the removal of dyes from wastewater. They include physical, chemical and biological processes such as liquid-liquid extraction, photodegradation, ion exchange, membrane filtration, electrochemical treatments, coagulation-flocculation and adsorption. [7,8] Among the above processes, adsorption is considered one of the best alternative and economically attractive methods for wastewater treatment due to its convenience, easiness of use, simplicity of design and efficiency. [9]

Different types of sorbents have been developed and applied for the removal of dyes from water such as clays, activated carbon and its derivatives, polysaccharides and natural and synthetic polymers. [10-13] An effective adsorbent must be nontoxic, regenerable, and easily applicable to the used technology. The efficiency of the adsorption process is closely related, respectively, to the physicochemical properties of the adsorbent (specific surface area, particle size, pore volume, zero charge point, bulk density and the presence of various functional groups on the surface of the adsorbent) as well as to the parameters used during the adsorption process (pH, temperature, contact time). [14] Adsorbent

recovery from treated media is a major issue in water treatment technology. Tedious filtration and centrifugation steps using energy-intensive pumping are often required to accelerate liquid flow through the filters. [15]

In recent decades, particular attention has been focused on the use of magnetic adsorbents, especially iron oxide adsorbents, in the field of environmental sciences. [16, 17] Moreover, the functionalization of their surface will facilitate the attachment of a large number of ions or charged mole-cules. [17, 18] These compounds have unique magnetic properties, as they are often superparamagnetic, and can thus be easily manipulated and separated by an external magnetic field without the need for filtration/settling or centrifugation steps, following the decontamination process. Magnetic nanoparticles (MNPs) also exhibit remarkable properties compared to their bulk analogues such as biocompatibility, low toxicity, good stability and high specific surface area which results in limited internal diffusion resistance leading to high adsorption capacity. [19]

An explored route to develop magnetic adsorbents from hydrogel beads is to encapsulate MNPs within lattice frameworks. [20, 21] Indeed, encapsulation is an economical and environmentally friendly process to immobilize a material in a hydrogel matrix, while maintaining its own properties. These uniformly sized gel beads offer advantages not only due to the high content of active components, but also for their ability to be used in a batch reactor. After saturation, the desired magnetic properties of these hydrogel beads give them the advantage of being magnetically separated from the effluent to be treated.

Carboxymethyl cellulose (CMC) is one of the most abundant polysaccharide derivatives in nature and has been widely used as an adsorbent in aqueous solutions due to its low cost of preparation, biodegradability and lack of tox-icity. [22] In addition to their non-negligible adsorption capacity, CMC are interesting owing to their properties to form gels in the presence of trivalent cations such as aluminum or iron ions. [23,24]

Previously, we reported the optimization study of simple CMC beads as well as semi-interpenetrating network composite beads CMC-Dextran sulfate and their application for the adsorption of methylene blue (MB) dye. [25,26] The latter showed remarkable MB removal efficiency, which was attributed to the additional functional groups of dextran sulfate as well as their convoluted structure with more pores and cavities. In this study, we proposed magnetic CMC/Dextran sulfate nanocomposite beads enclosing Fe3O4 nanoparticles modified with citrate ions, which can not only promote the adsorption and recovery of cationic dyes, but also has the advantage of being easily separated from the medium. The modification of the nanoparticles was performed to ensure the stability of its suspension while improving its adsorption properties through citrate carboxylate ions. Our objective was to develop an original material that could be integrated into a water treatment process by taking advantage of the magnetic aspect of the beads for their extraction from the medium to be depolluted. To be part of an eco-design approach, the matrix of the beads is based on natural polymers that constitute “millicapsules” in which the MNPs are stored. The aim was to take profit of the magnetic and adsorbent properties of the nanoparticles while confining them in the polymer matrix to avoid their dispersion in the environment and thus to alleviate the problem of nanomaterial toxicity. On the other hand, the incorporation of these nanoparticles in the beads reinforces their mechanical and thermal properties. The prepared hydrogel materials were tested as adsorbents for the removal of MB pollutant. The influence of Fe_3O_4 nanoparticles on the structure and swelling properties of nanocomposite beads were also investigated. In summary, this work represents a continuation of the previous studies carried out on this type of material[25,26] to achieve a comprehensive study and overcome the shortcomings encountered previously such as the poor mechanical and thermal stability of the CMC/Dextran sulfate matrix.

2. Materials and methods

2.1. Materials and chemicals

CMC sodium salt (CMC, Mw ~700 kDa, DS ~ 0.9, viscosity 2500 — 6000 cps (1% in H_2O at 25 °C), sodium (Na) content 6.5 — 9.5%), Dextran sulfate sodium salt (DS, Mw 7-20 kDa, sulfur content (S/C-analysis) 17.0 — 19.0%) were purchased rom Sigma-Aldrich Co. Ltd. (St. Louis, MO). Aluminum nitrate nonahydrate ($Al(NO_3)_3.9H_2O$), sodium n-dodecyl sulfate (SDs), MB ($C_{16}H_{18}ClN_3S$), sodium citrate ($Na_3C_6H_5O_7$), sodium chloride (NaCl), sodium hydroxide (NaOH), ferric chloride hexahydrate ($FeCl_3.6H_2O$) and ferrous sulfate heptahydrate ($FeSO_4.7H_2O$) were received from Sigma-Aldrich. Other chemicals of analytical grades, ethanol and acetone, nitric acid, and citric acid, were used without purification. Doubly distilled water (DDW) was used for solution preparations.

2.2. Synthesis of magnetic and functionalized nanoparticles

Nanoparticles of magnetite (Fe_3O_4) were firstly synthesized by conventional co-precipitation of a stoichiometric mixture of ferrous and ferric salts (mole ratio 2:1) in alkaline medium.[27] Briefly, $FeCl_3.6H_2O$ and $FeSO_4.7H_2O$ were dissolved all together in DDW under vigorous stirring at 80 °C. Then, NaOH solution (2M) was added dropwise to the mixture maintained at pH11 for 30 min, and where a black precipitate was progressively appeared. The nanoparticles Fe_3O_4 thereby formed (MNPs) were separated by a magnetic external field, washed several times with DDW, and then dried in oven at 80 °C for 24 h.

In second step, nanoparticles surface was modified by citrate ions to obtain stable functionalized magnetite. For this end, the weighted MNPs (2 g) were dispersed in 150 mL of citrate solution (0.5M) at 80 °C under mechanical stirring for 1 h, and then the suspension pH was adjusted to 5 by nitric acid solution (1M). Afterward, the modified nanoparticles (m-MNPs) were collected by external magnetic field, washed with DDW, and dispersed again in 100 mL of citric acid solution (0.2M) under stirring for further 2 h. Subsequently, m-MNPs were treated in acetone to remove excess of hydrogen (H^+)[**28**] followed by washing thoroughly with DDW and drying in oven at 80 °C for 24 h.

2.3. Preparation of magnetic nanocomposite beads

Magnetic semi-interpenetrating hydrogel nanocomposite beads were prepared at room temperature from CMC and DS incorporating MNPs at different contents via ionotropic gelation method according to our previous works with some modifications.[25,26]

Aqueous solution mixture was obtained by dissolving required amounts of CMC (1.5% w/v), DS (0.75% w/v) and SDS (0.2% w/v) in 100 mL of $NaCl$ solution (4% w/v) under vigorous magnetic stirring (400 rpm) for 2 h. Then, $m-MNP$s was added to the former solution at various contents x (w/w with respect to CMC) and keep under mechanical stirring for another 1 h. The obtained viscous mixture was then extruded through a hypodermic syringe needle into 200 mL of crosslinker $Al(NO_3)_3.9H_2O$ solution (3% w/v) under gentile magnetic stirring. The obtained spherical and homogeneous beads were stirred for another 30 min, and subsequently left overnight at 4 ° C for hardening. The wet beads were collected, washed thoroughly with DDW, followed by ethanol/water mixture (8:1 v/v) for several times to eliminate surfactant,[29] and then dewatered in ethanol for 24 h. At last, they were dried in oven at 60 °C, and stored for later use. The as-prepared magnetic beads were designated m-MNPsx-C/D0.5 with x = 0.3, 0.4, 0.5.

For comparison, unmodified magnetite $MNPs$ were as well incorporated at a fixed ratio ($x = 0.4$) to obtain magnetic MNPs0.4-C/D0.5 beads according to the same procedure.

Likewise, virgin beads without $MNPs$ were prepared as control sample and referred as MNPs0-C/D0.5.

The amount of Al^{3+} cross-linking agent as well as iron ions within the beads were determined by Inductively Coupled Plasma Mass Spectrometry (ICP-MS) after mineralization of the samples by acid attacks. Briefly, 1 g of beads was treated with 50 mL of hydrochloric acid (5M) at 80 °C for 1h. The result was expressed as mg of ions per g of beads (mg g^{-1}).

2.4. Characterization

The chemical structure of raw materials, magnetic NPs and their nanocomposite beads were characterized by ATR-FTIR (Bruker Vector 22 FTIR Spectrometer GmbH, Germany) in the range of 400-4000 cm^{-1}. X-Ray diffraction patterns were recorded on Bruker D8 Advance A 25 X-ray diffractometer using CuKa as the source in the range of 10-70°. A Nova NanoSEM 450 (FEI Europe, Eindhoven, Netherlands) instrument with Schottky field emission electron beam (impact energy of 0.02 to 30 keV) was used to analyze the magnetic NPs and the fractured surfaces of Freeze-dried beads. SEM images were performed under high vacuum conditions on the dried samples without metallization or other treatment. Elemental composition of the samples was provided by an EDX accessory coupled to above SEM. The size distribution of $MNPs$ before and after modification by citrate ions was estimated via Zetasizer Nano ZS (Malvern, UK) instrument at 27 °C and scattering angle of 173°. To study the magnetic properties of magnetic adsorbents, a vibrating sample magnetometer (VSM 7407) was used with an applied static field of — 10kO_e to +10kO_e. Thermal degradation of the samples was performed using a TGA Q500 (TA Instruments, New Castle, DE) by heating from 40 to 580 °C under a nitrogen atmosphere at a rate of 10 °C min-1. ICP-MS was conducted on Agilent 7700x ICP-MS model (USA) in argon (0.35 L min^{-1}).

2.5. Swelling measurements

The swelling behavior of hydrogel beads were investigated in DDW and different pH solutions to assess their water retention ability. Pre-weighted dry samples ($W_d = 0.10$ g) were immersed in excessive DDW of varying pH (2, 4, 6, 7, 8, 10 and 12) and equilibrated for 24 h. The soaked samples were collected, wiped with tissue paper and weighed (W_s). The results were an average of three tests. The swelling ratio (SR) (g g^{-1}, (%)) were then calculated by using Equation (1).

$$\mathrm{SR}(\%) = \frac{W_s - W_d}{W_d} \times 100 \qquad (1)$$

2.6. Point zero charge (pH_{PZc}) determination

The point of zero charge (pH_{PZC}) of the magnetic nano-biocomposite hydrogels were determined using the Cerovic method.[30] Briefly, 0.1 g of the hydrogel was immersed into 25 mL of aqueous KNO_3 solution (0.01M) at different pH ranging from 2 to 12 for 24 h. The final pH_f of the solutions was

measured by an electronic handheld pH meter DELTA-320 (accuracy $\pm$ 0.1). The pH_{PZC} values (at $\Delta pH = 0$) of each sample was determined from a plot of the DpH ($pH_i - pH_f$) versus pHi.

2.7. Adsorption study

Batch adsorption process was carried out to investigate the adsorption of by the magnetic nanocomposites' beads. Experiments were performed in single reactor systems with five independent parameters, namely adsorbent dose (0.5-6g L^{-1}), solution pH (2-12), contact time (5-720 min), initial dye concentration (50-1500 mg L^{-1}) and temperature (25-55 °C). After adsorption, samples were removed from the dye solution using a magnet and the remaining concentration of MB was evaluated using a UV visible spectrophotometer (VWR (UV-3100PC)) at 664 nm. Each experiment was carried out in triplicate and the average value was considered. The adsorption capacity and the removal efficiency R (%) were calculated using the following Equations (2) and (3), respectively.

$$q_t = \frac{C_0 - C_t}{m} \times V \qquad (2)$$

$$R\ (\%) = \frac{C_0 - C_t}{C_0} \times 100 \qquad (3)$$

where q_t is the adsorption capacity at time t, m is the weight of the adsorbent (g) and V is the volume of the solution (L).

2.8. Regeneration study

Regeneration studies are essential for reuse of the adsorbent in continuous batches. Desorption of MB from dyes-loaded magnetic beads was performed via batch method in 0.5M NaCl solution of water/ethanol (50/50 v/v) according to our previous works.[25,26,31] After elution of dye, the regenerated beads were washed with DDW and dried in an oven before reused in the next adsorption/de-sorption cycle. Then, the recycling efficiency in each cycle was estimated (Equation (4)). The reuse cycles were repeated for five times.

$$\text{Desorption } \% = (\text{Desorption/Adsorption}) \times 100 \qquad (4)$$

3. Results and discussion

3.1. Formation and stability of Fe_3O_4 nanoparticles in suspension

In this study, the stability of Fe_3O_4 was ensured by their functionalization with citrate ions. **Figure 1(a)** shows the pH_{PZC} determination curve of $MNPs$ as well as the photograph of $m - MNPs$ dispersed in DDW. The obtained pH_{PZC} was determined to be 7.33, in agreement with the magnetite value given in

the literature.[32] Furthermore, the functionalization of nanoparticles with citrate ions (pKa of $\sim$ 3.1, 4.8 and 6.4) leads to an improved stability of functionalized $m-MNP$s nanoparticles in suspension. Indeed, the appearance of the $m-MNP$s suspension was clear without any turbidity (as inset in **Figure 1(a)**) confirming the stability of these nanoparticles in suspension. Subsequently, the addition of the $m-MNP$s to the CMC/DS aqueous mixture at pH $\sim$ 7 leads to very stable suspensions for the syntheses of magnetic beads.

The powdery samples observed by SEM (**Figure 1b**(i)) are spherical and nano-sized with narrow distributions for both citrate-coated (100-115 nm) and uncoated (108-126 nm) magnetite nanoparticles, which provides maximum hypersensitivity to weak magnetic fields.[33] Moreover, the decrease in the size of citrate-loaded nanoparticles compared to unloaded particles is probably due to the fact that citrate acts as a masking agent that promotes the dispersion of the magnetite particles so produced and prevents their aggregation, thus increasing the specific surface area and the number of active sites obtained.[28] On the other hand, the average sizes of MNPs and m-MNPs determined from the DLS spectra (**Figure 1b**(ii)) are 334 and 178 nm, respectively. These values are higher than those found by SEM analysis especially for unmodified nanoparticles, which is probably due to the aggregation of these samples in suspension during DLS analysis.[34] EDX spectrum of the nanoparticles (**Figure 1b**(iii)) shows the peaks of iron and oxygen elements with predominant compositions. The functionalization of these nanoparticles by citrate ions was confirmed in the $m-MNP$s spectrum by the coexistence of carbon and sodium peaks from the modifier salt.

3.2. Preparation of magnetic beads

The suggested crosslinking process and preparation procedure of the magnetic hydrogel beads are illustrated in **Figure 2(a)**. According to the literature, this class of so-called ionotropic hydrogels are stabilized mainly by electrostatic interactions. Indeed, following a cationic exchange with Na+ ions, each Al^{3+} ion provides a bridge between three CMC chain ends at the carboxylate groups. In addition, it could be seen that the swollen beads were spherical with an approximate millimeter diameter of about 3 mm for the MNPs0-C/D0.5 matrix and 3.5 mm for the magnetic beads. However, after drying, their diameter was considerably reduced to about 1.2 mm and during the swelling tests; the initial size was not recovered. We could therefore deduce that a partial closure of the pore volume and collapse of the alveolar structure occurs, which we attribute to the evaporation of the residual liquid in the beads during drying. The retention of nanoparticles within the magnetic beads was evidenced by the gray color of the beads as well as the transparency of the solutions from the cross-linking and washing steps. Also, the addition of the SDS surfactant in the presence of NaCl before the extrusion process leads to the formation of stable spherical micelles which act as a template for interconnected pores formation.[25,26]

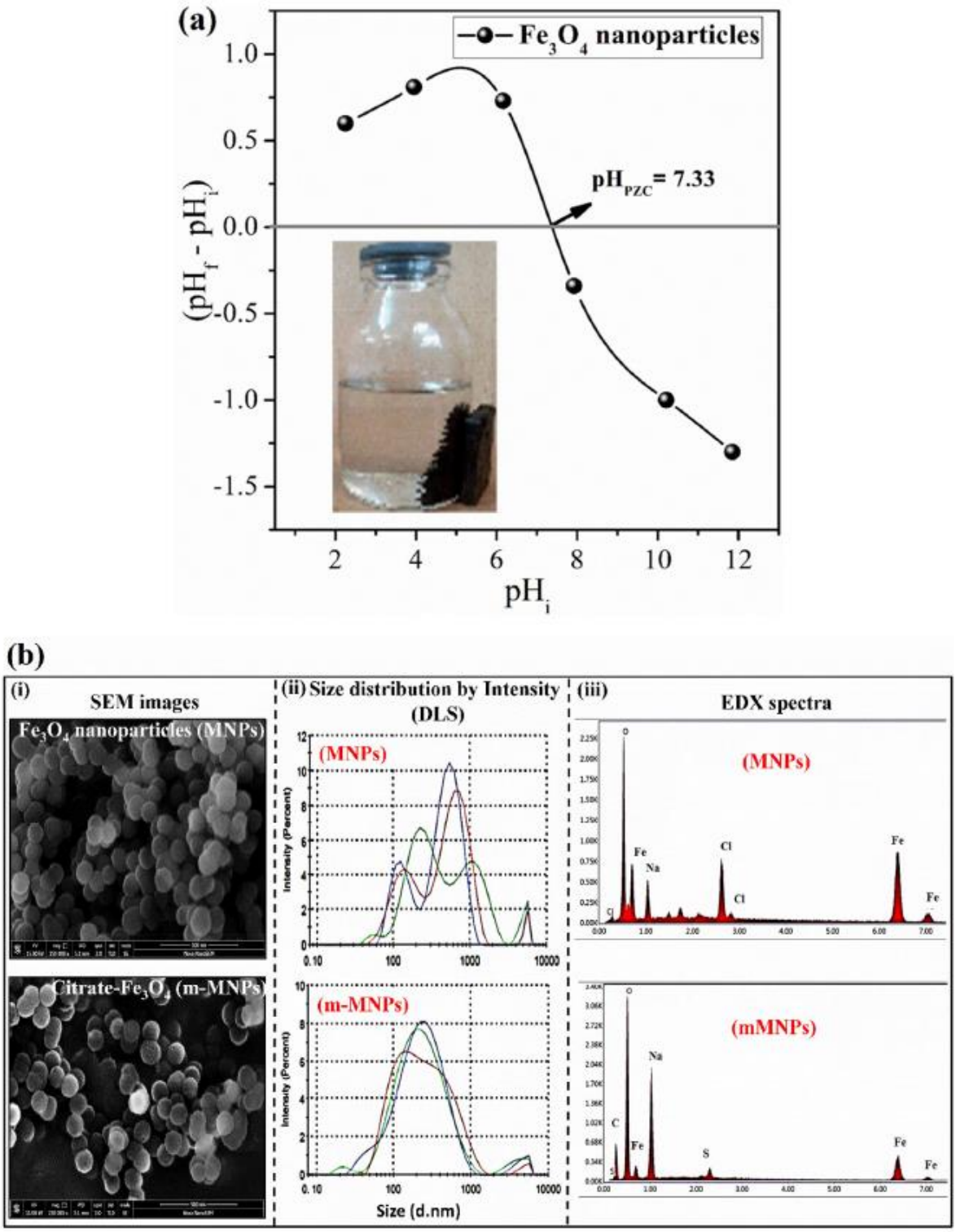

Figure 1. (a) pH_{PZC} Determination of ($MNPs$) magnetic nanoparticles and photograph of dispersed citrate-loaded nanoparticles $m-MNPs$ (as inset), (b) The corresponding SEM micrographs (i), DLS (ii) and EDX spectra (iii).

Figure 2b(i) shows SEM micrographs of oven-dried bead surfaces as well as cross sections of freeze-dried counterparts for both systems with and without magnetic nano charge. As it can be seen, for all samples, the obtained hydrogel beads exhibited relatively rough and compact external surfaces and an interconnected microporous structure with welldefined interstices. The introduction of $MNPs$ generated a clear restriction in the size of the micropores and the thickness of its walls from (140-170

im) to (10-50 μm). In addition, the loaded beads exhibit larger sizes compared to the unloaded ones. This fact, associated with the high porosity as well as the roughness of the structure could probably lead to an increase in their specific surface areas, and thus improve their capacity to adsorb the MB dye. On the other hand, the appearance of the iron peak in EDX spectra of magnetic beads attested the successful encapsulation of magnetite nanoparticles (**Figure 2b**(ii)).

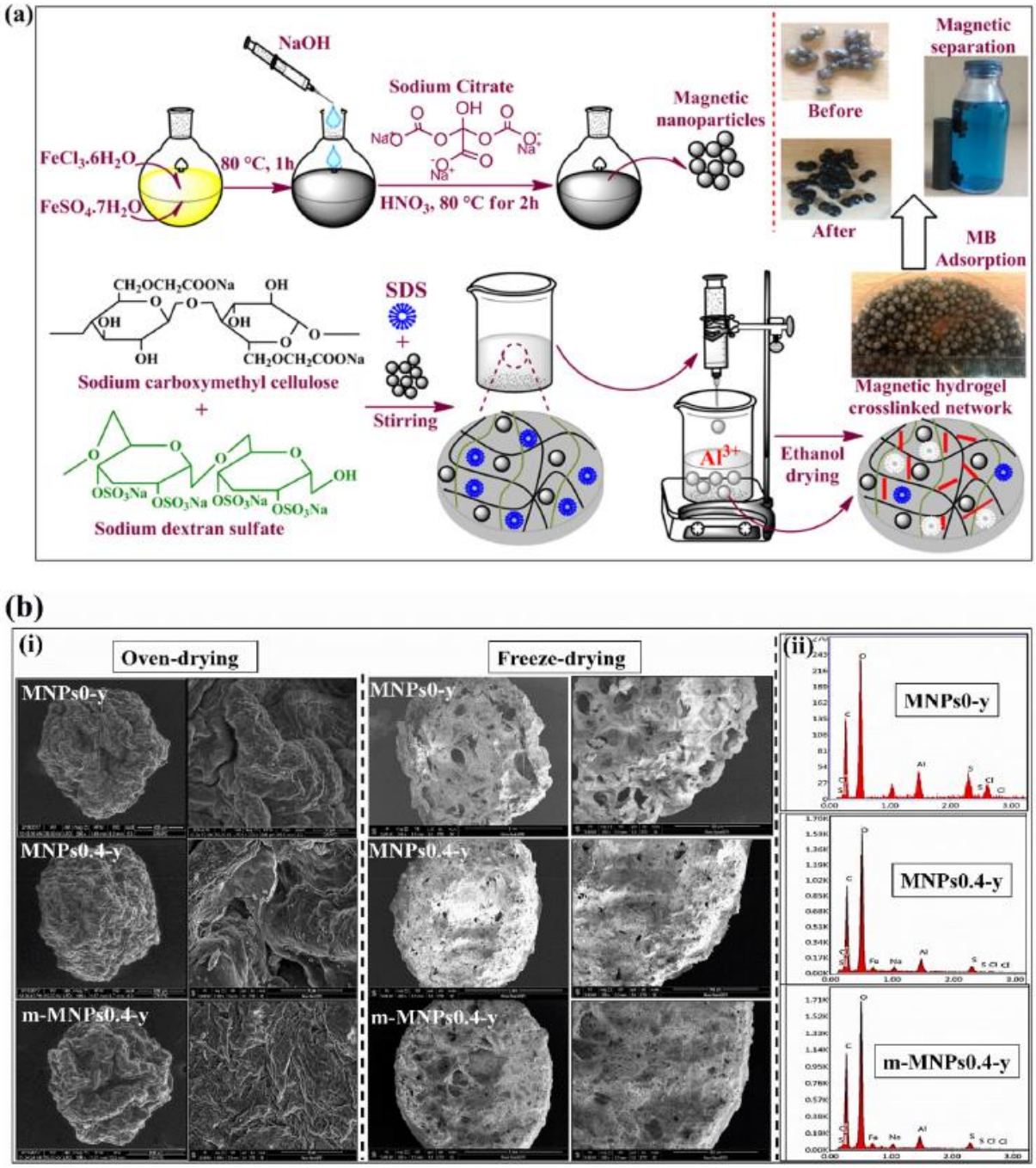

Figure 2. (a) Graphic steps for the preparation of nanocomposite hydrogel beads and its application, (b) SEM micrographs of beads observed after oven-drying and freeze-drying (i; with y = C/D0.5); the corresponding EDX spectra (ii).

Figure 3(a) displays the XRD patterns of citrate-loaded ($m-MNPs$) and unloaded ($MNPs$) $MNPs$. As observed, both samples present the main characteristic peaks of polycrystalline magnetite (PCPDFWIN v.2.02, PDF no. 85-1436) at approximately the 2h of 30.3°, 35.5°, 37.27, 43.2°, 53.5°, 57° and 62.7° with

Miller indices of (220), (311), (222), (400), (422), (511) and (440), respectively.[35] This result indicates that the crystal structure was not altered after MNPs functionalization. The average sizes of the pure magnetite nanoparticles and those coated with citrate were determined respectively at 192 and 180 nm using the Scherrer's formula at the most intense diffraction plane (311).[36] These values are close to the mean sizes calculated by SEM analysis. From **Figure 3(b)**, the XRD pattern of the matrix shows no diffraction peaks, indicating the amorphous nature of both polysaccharides (CMC and DS). However, those of the nanocomposites display the characteristic peaks of Fe_3O_4 nanoparticles, suggesting that their crystal structure was not altered after their encapsulation within the beads.

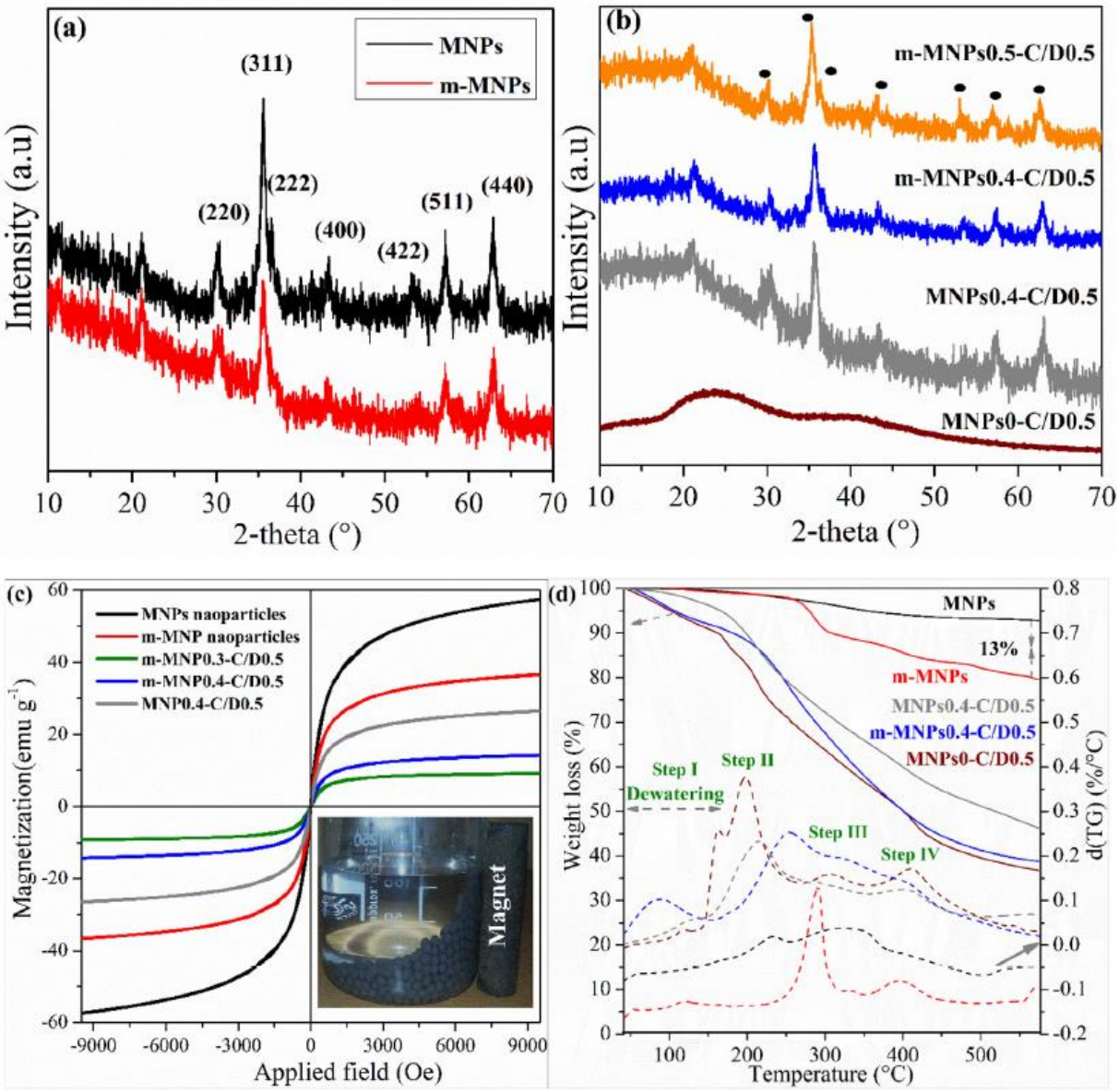

Figure 3. XRD patterns of (a) MNPs and $m-MNP$s nanoparticles; (b) Pristine hydrogel and its nanocomposites; (c) Its hysteresis loops (inset: magnetic separation of the sample) and (d) TGA/d(TG) thermograms.

Table 1. Magnetic properties of $MNPs$ and $m-MNPs$ nanoparticles and their magnetic hydrogel beads.

Sample	SMV (emu g^{-1})	Mr (emu g^{-1})	Hc (Oe)
MNPs	57.47	0.92	11.79
m-MNPs	36.24	0.61	10.63
MNPs0.4-C/D0.5	26.52	0.61	12.58
m-MNPs0.3-C/D0.5	9.21	0.49	28.83
m-MNPs0.4-C/D0.5	14.09	0.33	12.54

Same results were found for chitosan-g-(2-acrylamido-2-methyl propanesulfonic acid)/(acrylic acid)/magnetite,[37] Fe_3O_4/chitosan/$Al(OH)_3$[38] composites as well as magnetic polydopamine/polycarboxylic.[39]

The magnetic behavior of the samples was performed using VSM analysis at $\pm$ 10 kO_e and the obtained data are given in **Figure 3(c)** and **Table 1**. The saturation magnetization values (SMV) of the two nanoparticles $MNPs$ and m-MNPs obtained at room temperature were 57.73 and 37.33 emu g^{-1}, respectively. This difference in SMV is mainly associated to the chemisorption of citrate ions on the surface of Fe_3O_4 nanoparticles. Tang et al. have and Verma et al. found similar observations in the case of magnetic materials coated with tetra-ethylene-pent-amine and glycine, respectively.[40,41] Otherwise, the MNPs0.4-C/D0.5, m-MNPs0.3-C/D0.5 and m-MNPs0.4-C/D0.5 magnetic hydrogel beads show lower SMV values than the $MNPs$ (**Table 1**). This behavior indicate that these values are markedly affected by the number of nanoparticles enclosed within the crosslinked hydrogels and the surface effects generated by the coating of nanoparticles with CMC and DS chains having non-magnetic properties. Also, the values of remanent magnetization Mr and coercivity Hc almost zero for nanoparticles and magnetic beads testify superparamagnetic behavior.[42] The inset photographic in **Figure 3(c)** reveals that the magnetic beads can be easily and completely separated from the dye solution with the external bar magnet, suggesting that the magnetic beads have a relatively good magnetic power.

TGA analysis was carried out to evaluate the loading amount of citrate molecules on the surface of M nanoparticles and to investigate the effect of the latter on thermal stability of the prepared hydrogels. The TGA/DTG curves of $MNPs$, $m-MNPs$, the matrix hydrogel and its magnetic nanocomposites were presented in **Figure 3(d)**. As observed, M displays two degradation steps with mass losses and associated T_{max} of 2.3% at 230 °C and 3.53 at 326 °C, which corresponds to the removal of physisorbed water and dehydroxylation of surfaces.

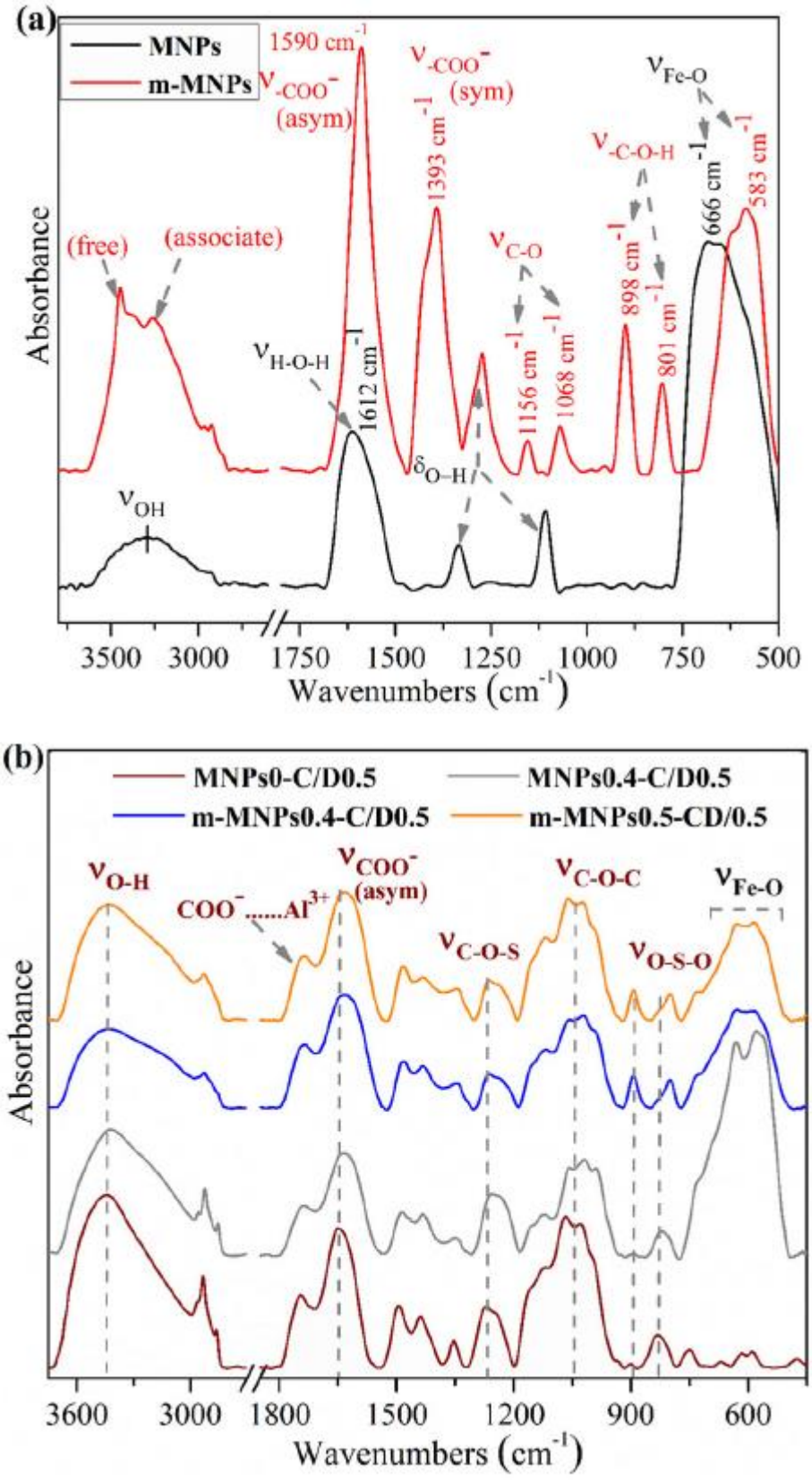

Figure 4. $FTIR$ spectra of (a) unmodified and modified nanoparticles; (b) The MNPs0-C/D0.5 matrix and its nanocomposites.

Furthermore, a third degradation step occurs above 500 °C which can be attributed to the phase transition of nanoparticles from magnetite (Fe_3O_4) to hematite (Fe_2O_3).[43] The total mass loss at 570 °C was estimated to be 7% being iron oxide the only residue. Otherwise, citrate-loaded nanoparticles $m-MNP$s was degraded in three distinguished steps. The first one was due to the dehydration of the sample (T < 150 °C). The second stage with a mass loss of 10.4% (T_{max} of 290 °C) is attributed to the elimination of the free sodium citrate molecules adsorbed on the surface. Zhao et al. also observed the same behavior in their study based on the functionalization of Fe_3O_4 nanoparticles by oleic acid.[44] The third decomposition step (350 < T < 500 °C) was the result of the degradation of the stable residual products from the previous steps (Δm = 6.23%). According to the total mass loss, the amount of citrate molecules anchored to the MNPs surface was estimated to be about 13% (130 mg g^{-1}). This suggests the formation of coherent chemical bonds between the citrate ions and the MNPs nanoparticles.[45]

In the other hand, magnetic hydrogel beads underwent several thermal processes similar to those of the matrix previously reported,[25,26] including the desorption of physically adsorbed and structural water (first step: $T \leq 200$ °C), depolymerization by breaking the $C-O$ and $C-C$ bonds in the ring units (second and third step: $200 \leq T \leq 360$ °C) with release of volatile products (CO, CO_2 and H_2O) and lastly the carbonization of the residues from the previous steps (360-575 °C). However, nanocomposite hydrogels show a few slight changes. Thus, an improvement of the stability was observed at the second and third steps, which is justified by an increase of the Tmax values from 196 °C for the matrix to reach 214 and 250 °C for MNPs 0.4-C/D0.5 and m-MNPs0.4-C/D0.5 observed for the second step, respectively. This finding may also be explained by an overlap of the former steps II and III for nanocomposites. An inverse effect was found at the third step, which reveals that the depolymerization of the network chains is slightly accelerated following the incorporation of MNPs and m-MNPs nanoparticles. Lastly, all these observations reveal that the presence of MNPs leads to an improvement on thermal stability of nanocomposite hydrogels through a barrier effect induced by these nanoparticles. The last, may increase the cross-linking density by secondary interactions that restrict the mobility of molecular chains, leading to an improvement of the thermal stability.[46] Indeed, the matrix hydrogel (MNPs0-C/D0.5) presents a final residue of 38.85% of its total weight at 570 °C; whereas, at the same temperature, the residue is about 41.02% and 46.50% for m-MNPs0.4-C/D0.5 and MNPs0.4-C/D0.5.

The $FTIR$ spectra of the precursor components and prepared hydrogel beads are provided in **Figure 4**. For MNPs nanoparticles (**Figure 4(a)**), the broad bands at 668 cm^{-1} and 3305 cm^{-1} relate to Fe-O and O-H stretching vibra-tions.[47] MNPs hydration was confirmed by the band at 1612 cm^{-1} related to the deformation vibrations of H-O-H. Otherwise, the m-MNPs spectrum displays the presence of additional bands besides those of Fe_3O_4. The asymmetric and symmetric vibration bands of the citrate carboxylate groups appeared respectively at 1590 and 1393 cm^{-1}, indicating a bridging bidentate interaction. This result suggests a chemisorption of citrate ions on the surface of the nanoparticles via their carboxylate ions. Similar results has been reported by Verma et al. and Na et al.[40,45] Also, Fe-O band shift toward low wavenumbers by around 80 cm^{-1}, reflecting a chemical change in their environment due to the bonds established between surface oxygen atom and citrate -COO-.

On the other hand, the different characteristic bands of the pure compounds (CMC and DS) that have already been reported in our previous studies can be identified in all the cross-linked hydrogels spectra (**Figure 4(b)**).[25,26] The bands in the range 3300-3400 cm^{-1} are ascribed to OH stretching vibrations of CMC and DS backbone. The sharp bands at 1413 cm^{-1} and 1609 cm^{-1} are related to the asymmetric and symmetric $C = O$ vibrations of CMC carboxylate groups, while the broad band around 1040 cm^{-1} results from the CO vibrations of the carboxymethylation and C-O-C/C-O-S of CMC/DS matrix. In

addition, the characteristic bands of the DS sulfate groups are located at about 1240 cm^{-1} (asymmetric S = O stretching vibrations of the $O = S = O$ groups) and 830 cm^{-1} (asymmetric $S - O - S$ stretching vibrations in the -O-SO3- groups). Otherwise, the incorporation of MNPs in hydrogel beads generates a shift of certain peaks. Among them, the carboxylate and sulfate bands attributed to the asymmetric vibrations of COO- and -O-SO_3- vibrations that shifted by about 23 and 30 cm^{-1} in the presence of $MNPs$ and m-MNPs nanoparticles. These results suggest hydrogen-bonding occurrence between these groups and hydroxyls of the nanoparticle surfaces. Similarly, the band of the DS located at 605 cm^{-1} underwent a significant intensification, which reflects its overlap with that of the $Fe - O$ bonds. Furthermore, for m-MNPs-C/D0.5 nanocomposites, we observed the appearance of a weak peak at 890 cm^{-1} that was attributed to $C - O - H$ deformations from citrate ions.[48]

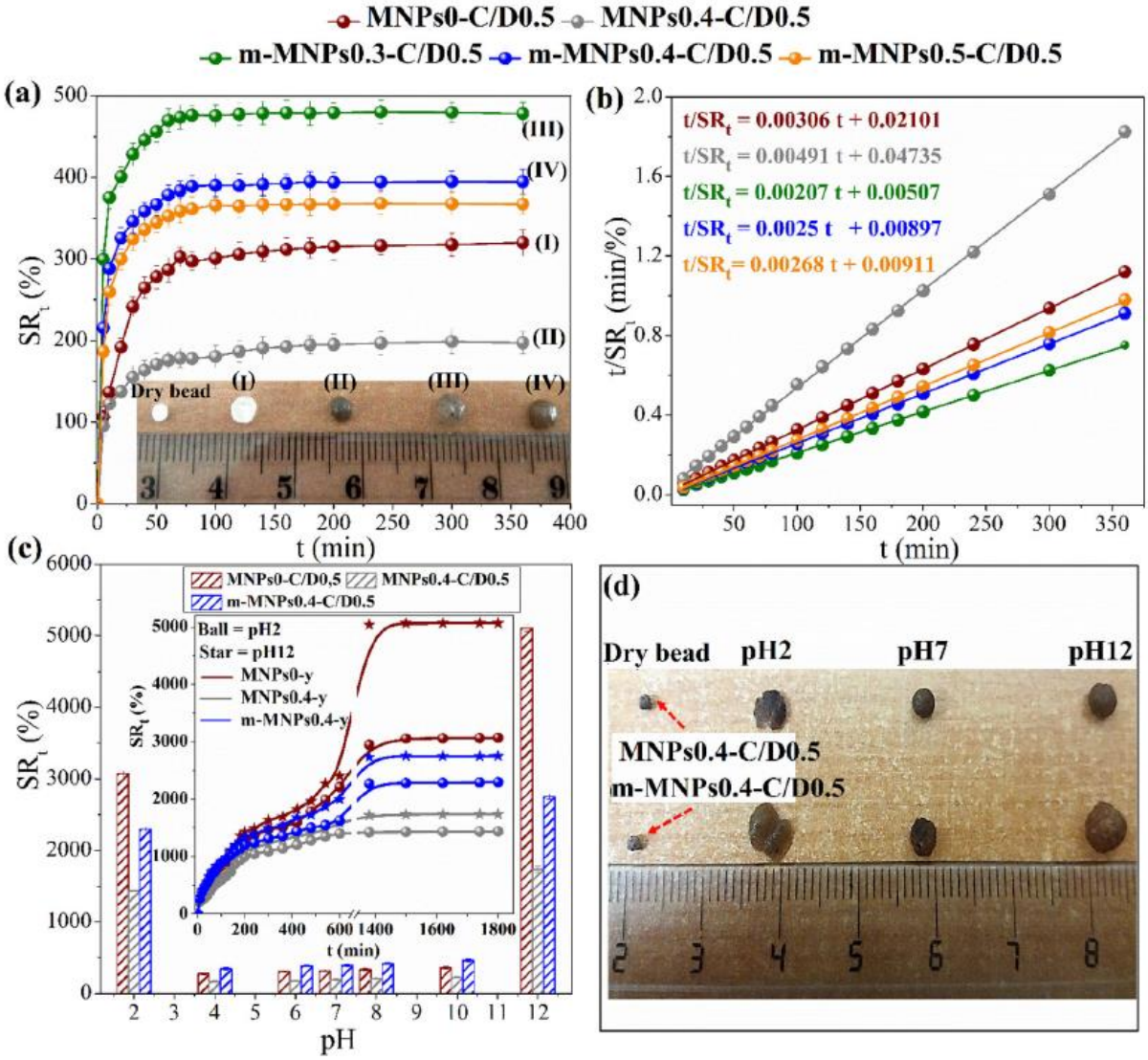

Figure 5. (a) Swelling kinetic curves of the prepared hydrogel beads; (b) Schott's pseudo-second order kinetic model plots; (c) pH sensitivity and (d) Photograph of the swollen beads in different pH media (y = C/D0.5).

3.3. Swelling capability and pH-sensitivity study

To further probe the water absorption capacity of the prepared hydrogels, the swelling kinetics of the hydrogels at different pH conditions were performed and the results are shown in **Figure 5**. As can be seen, the swelling behavior was observed to be similar for all hydrogels due to the presence of

hydrophilic groups such as hydroxyl, carboxylates and sulfates in their structure: it increases sharply in the first few minutes and then slows down until it reaches an equilibrium stage. However, the presence of $MNPs$ in the MNPs0.4-C/D0.5 magnetic hydrogel leads to an obvious decrease in SRs. This behavior can be attributed to an increase in the cross-linking density of the hydrogel beads as a result of secondary interactions between the polymeric chains and the $MNPs$, reducing the elasticity of the network.[20,49] On the other hand, an opposite effect was noticed in the presence of $m-MNPs$ within the m-MNPsC/D0.5 beads, which generate a remarkable increase in swelling ability as evidenced by the inset photograph of the swollen beads for 24 h (**Figure 5(a)**). Indeed, the equilibrium swelling capacity of the matrix hydrogel increases from 326 (g g^{-1}, %) to an optimum of 483 (g g^{-1}, %) with the addition of 30% m-MNPs, beyond which a decrease in swelling is observed while remaining better compared to the matrix. Considering that higher ratio of $m-MNPs$ nanoparticles (40 and 50%) lead to a greater occupation of the interstitial volume, thus reducing the elasticity of the network and its absorption capacity. Otherwise, the remarkable improvement in swelling for m-MNPs-C/D0.5 compared to the matrix was probably due to further electrostatic repulsions established between COO^-/OSO_3^- charges of the matrix and the carboxylate groups present on the $m-MNPs$ surface originated from citrate ions, which induces greater stretching of the chains leading to the creation of more interspaces.[26]

The dynamic swelling behavior of magnetic hydrogel beads in neutral media was estimated using Schott's second order kinetic model[50] expressed as below Equation (5).

$$\frac{t}{\mathrm{SR}_t} = \frac{1}{k_{\mathrm{is}}} + \frac{1}{\mathrm{SR}_\infty} t \qquad (5)$$

where the formula $k_{is} = k_s\, SR_\infty{}^2$ is the initial swelling rate constant and k_s is the swelling rate constant. SR_t is the SR at time t and SR_∞ is the theoretical equilibrium swelling (in g g^{-1}).

Figure 5(b) shows straight plots with R^2 coefficients close to unity (≥0.999). Besides, a slight difference between the calculated equilibrium swelling (SR_∞ values and the experimental data was observed (**Table 1S**: see supplementary data). This confirms that the swelling of the prepared hydrogel beads is controlled by the relaxation of the polymeric chains in the hydrogel networks.[51] In addition, magnetic nanocomposites exhibit the highest Kis rate constants where the maximum value of 197.24 g $g^{-1}min^{-1}$ was found for m-MNPs0.3-C/D0.5 that is four times greater than that of the matrix MNPs0-C/D0.5.

The swelling behavior of the hydrogel beads in different pH solutions was studied and the results are shown in **Figure 5(c)**. As observed, even though the $MNPs$ and $m-MNPs$ ratio incorporated in the matrix was 40%, the obtained magnetic hydrogels show a similar behavior to that of the matrix which has been discussed in detail in our previous study.[26] As expected, all prepared hydrogels exhibited the highest swelling in the alkaline medium compared to the acidic solutions. Indeed, at acidic pH, the surfaces of $MNPs$ and $m-MNPs$ nanoparticles are protonated or positively charged which generates electrostatic attraction forces between these nanoparticles and the O-SO_3- sulfate groups carried by the DS chains which is mostly ionized over the whole pH range (the pKa of methane sulfonic acid is ∼2.5).[52] This behavior can increase the cross-linking density of the beads, and thus reduce the elasticity of the network and its absorption capacity. Likewise, the protonated functional groups (-COOH, O-SO_3H and -OH) of various components can also participate in the cross-linking of the network by hydrogen bonding. Meanwhile, at basic pH, the negative charges of both nanoparticles induce

electrostatic repulsions with the negatively charged (OH^-, $-COO^-$ and $O-SO_3^-$) groups on the hydrogel structure leading to easy penetration of water molecules[53-55].

On the other hand, a dramatic increase in swelling capacity in strongly acidic or basic solutions (pH2 and pH12) was observed as confirmed by the SR_e values grouped in **Table 1S** (see supplementary data). This behavior is closely related to the release of Al^{3+} cross-linking agent into the swelling medium which can be explained as follows; (1) cation exchange between H+ ions and some Al^{3+} ions at pH2 (2) formation of aluminum hydroxide $Al(OH)_3$ through the Al^{3+} cross-linking agent at pH12. This promotes the diffusion of some Al^{3+} ions and subsequently decreases the cross-linking density of the network causing a better water uptake. Nevertheless, it should be noted that these highly swollen hydrogel beads may have some limitations, including easy disintegration during use and poor mechanical stability in aqueous solution as reflected in the photograph of the beads at pH2 which are almost completely deteriorated (**Figure 5(d)**).

3.4. Adsorption properties of magnetic beads

3.4.1. pH effect and pH_{PZC} determination

The pH of the medium is an important factor in the adsorption process since it influences the surface properties of the adsorbent and the ionization/dissociation of chelating groups.[56] **Figure 6(a)** displays the effect of solution pH in the range of 2-12 on the adsorption of MB on the matrix beads and its magnetic nanocomposites. As can be seen, a slight variation in equilibrium adsorption capacity as a function of solution pH for all beads was spotted with an optimum at pH7. To further investigation of the pH impact on MB adsorption, the pH_{PZC} of both simple and magnetic beads were studied and discussed. The calculated pH_{PZC} were determined at $pH_{PZC} = 3.26$, 3.70 and 4.07 for MNPs0-C/D05, MNPs0.4-C/D0.5 and m-MNPs0.4-C/D0.5, respectively. According to literature, at $pH < pH_{PZC}$, the surface of the beads is positively charged while above this value, negative charges dominate. Indeed, at pH values $\geq pH_{PZC}$ (**Figure 6(b)**), all the beads become negatively charged, facilitating the interaction between the cationic dye and the functional groups on adsorbent surfaces (COO^-, $-SO_3^-$ and FO^-). In addition, the low adsorption values obtained above pH7 is probably related to the screening effect of counter ions (Na^+). Conversely, in acidic pH, the presence of excess H^+ ions causes protonation of the -COOH, $O-SO_3H$, OH and F-OH groups while competing with the MB cationic dye, which can contribute to a decrease in MB adsorption capacity. This finding is also corroborated by the low pK_a value of the matrix sulfate species, which occur almost in the ionized state over the entire pH range as previously indi-cated.[26] Analogous MB adsorption behavior by other adsorbents has been reported previously.[17,20,57] Regarding the effect of m-MNPs, the m-MNPs0.4-C/D0.5 composite displayed higher removal efficiency than the pristine hydrogel in the whole pH scale, which was attributed to the additional carboxylate sites that bind the dye molecules through electrostatic interactions. However, an opposite effect is observed in the presence of MNPs, which could be attributed to the consistency of the highly cross-linked MNPs0.4-C/D0.5 beads after incorporation of MNPs nanoparticles.

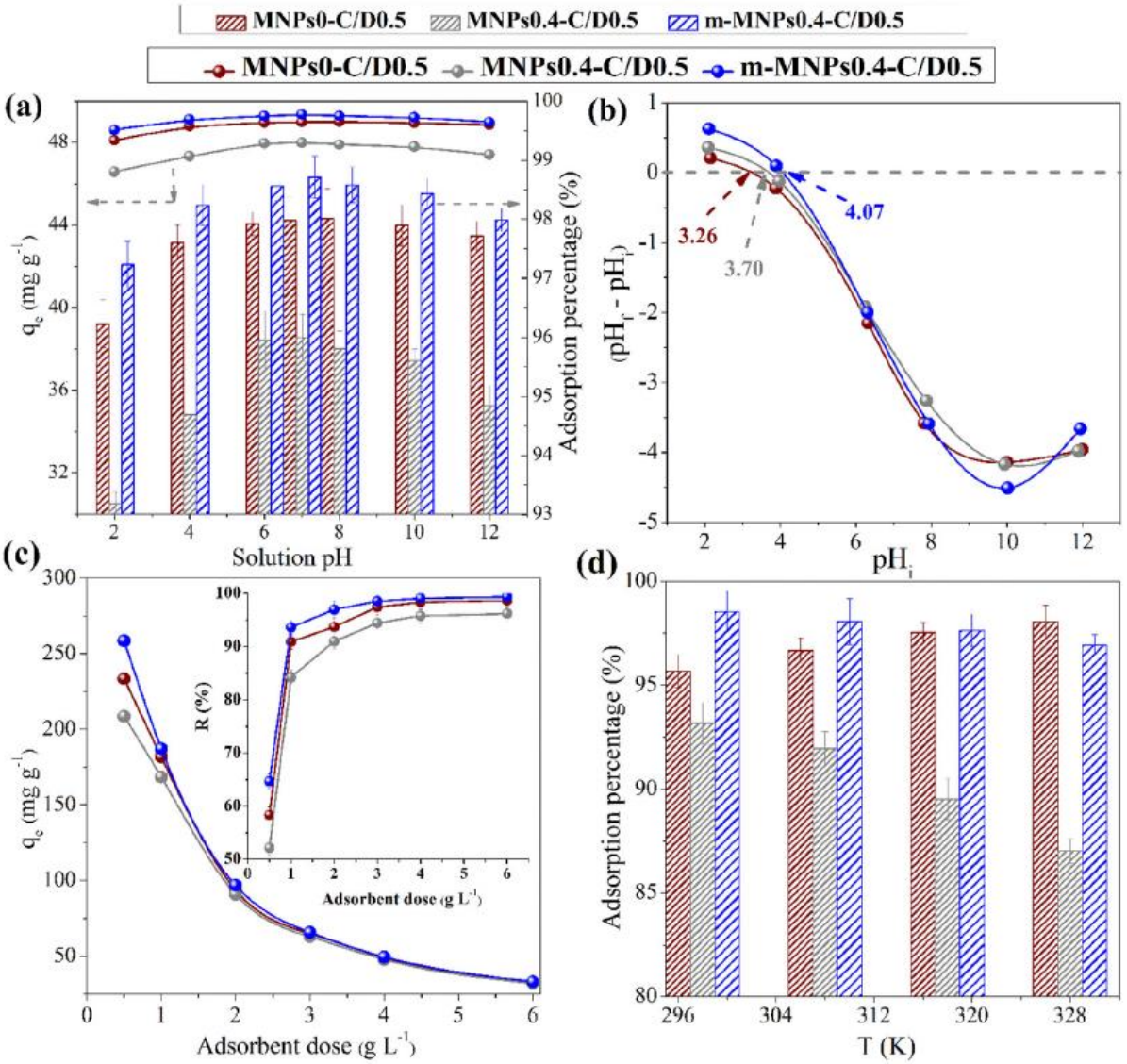

Figure 6. Effects of different adsorption parameters: (a) Initial pH solutions, (c) Adsorbent dose and (d) Temperature ($C_0 =$ 200 mg L^{-1} contact time of 5 h, adsorbent dosage of 1 g L^{-1}, temperature 25 °C, pH value of 7), (b) Ph_{PZC} determination using MNPs0-C/D0.5, MNPs0.4-C/D0.5 and m-MNPs0.4-C/D0.5 hydrogel beads.

3.4.2. Effect of adsorbents dose and temperature

Figure 6(c) illustrates the effect of the adsorbent dosage from 0.5 to 6g L^{-1} on MB adsorption of MNPs0-C/D0.5 and its magnetic hydrogels. Overall, all hydrogels exhibited similar behavior. The amount of adsorbed MB decreases sharply with increasing the dose of adsorbent from 0.5 to 6g L^{-1}. Simultaneously, the R (%) yield increases with the enrichment of the MB solution by adsorbent until it reaches a maximum at 1 g L^{-1}, reflecting the saturation of the adsorption sites.[25] This result can be easily explained by the differences in the number of active groups present either on the surface or in the internal bulk of the studied hydrogels. Additional amounts of adsorbent provide more available active sites which leads to an increase in the dye adsorption efficiency ($R\%$). However, the competitive effect between these groups for the binding of dye molecules decreases their adsorption capacities (q_e).

Figure 6(d) shows the effect of temperature in the range 298-328 K on MB adsorption efficiency of MNPs0-C/D0.5 matrix beads and its MNPs0.4-C/D0.5 and m-MNPs0.4-C/D0.5 nanocomposites. As revealed, increasing the temperature results in a slight decrease in the removal efficiency of both MNPs0.4-C/D0.5 and m-MNPs0.4-C/D0.5 magnetic beads, while an opposite effect was observed for the matrix. This means that a thermal increase reduce the interactions of MB molecules with the surface of the magnetic adsorbents, thus preventing their diffusion to the active sites.[58]

3.4.3. Effect of contact time and initial dye concentration on MB adsorption

The adsorption kinetics were studied to evaluate the equilibrium time required for MB adsorption onto unloaded and loaded-magnetic beads in the range of 0-720 min. According to the results shown in **Figure 7(a)**, the adsorption rate on all hydrogel beads increases significantly during the first few minutes and then gradually stabilizes nearing equilibrium.

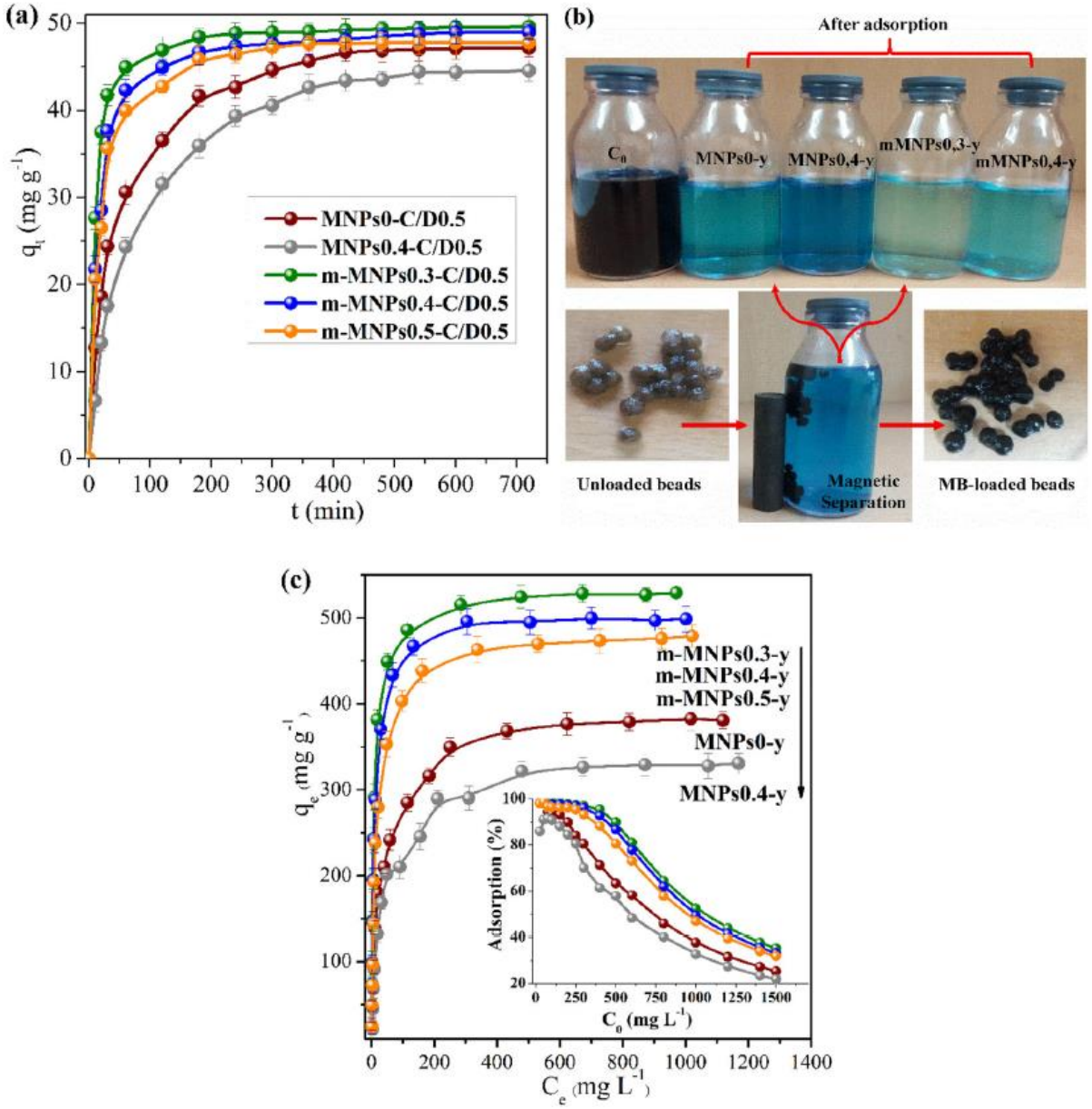

Figure 7. Impact of (a) contact time and (c) initial dye concentration on MB adsorption capacity of magnetic nanocomposite beads and their matrix, (b) photograph showing MB solutions and hydrogel beads before and after adsorption (y = C/D0.5).

The low adsorption rate observed over time was probably due to the fact that these active sites become saturated and less accessible by the dye molecules, which also suggests the existence of possible repulsive forces between adsorbed dye molecules and those in solution. The kinetic curves was monotonically continuous, suggesting a monolayer coverage of MB molecules on adsorbent surfaces.[59] Moreover, equilibrium was reached faster at about 3h for m-MNPs-loaded magnetic beads, while at 6h for those of MNPs-loaded and simple unloaded ones. Indeed, the removal efficiency R (%) obtained at 3h was about 83%, 72% and 92% for MNPs 0-C/D0.5, MNPs 0.4-C/D0.5 and m-MNPs0.4-C/D0.5, respectively, as shown in the post adsorption solutions image (**Figure 7(b)**). The high and fast adsorption observed for m-MNPs0.4-C/D0.5 may be attributed to the additional carboxylate and hydroxyl active sites of the m-MNPs citrate surfaces besides the anionic groups (carboxylates, sulfates) of CMC/DS polymers. Hence, MB molecules are easily adsorbed by these active sites via physical interactions (hydrogen bonding, van der waals and electrostatic interactions). Also, the porous structure observed by SEM and the higher swelling capacity of such adsorbents may facilitate the diffusion of MB molecules and promote a greater affinity toward the MB dye. It is worth mentioning that the m-MNPs0.3-C/D0.5 hydrogel has the greatest adsorption capacity compared to other nanoadsorbents. Beyond this optimum value of 30% m-MNPs, the removal capacity of MB decreases while remaining higher than that of the matrix. This may be due to the fact, that m-MNPs nanoparticles occupy progressively more internal pores, leading to a decrease in the specific surface area of m-MNPs-C/D0.5 magnetic beads and their adsorption capacity.

The effect of varying C0 on the removal efficiency (%) and adsorption capacity (qe) was investigated in the range 25-1500 mg L^{-1} at 1g L^{-1} of adsorbent dosage. From **Figure 7(c)**, the adsorption capacity of all adsorbents was improved with increasing dye concentrations until an equilibrium state is reached. Indeed, at low initial concentration, the availability of a sufficient number of active sites induces a random adsorption of MB molecules on the surface of the adsorbents. However, at high concentrations, the driving force due to the concentration gradient is greater,[60] resulting in significant MB adsorption. Simultaneously, the removal (%) decreases significantly at higher $C0$ values (as inset in **Figure 7(c)**), which can be explained by the decrease in active sites at higher dye concentrations and the concurrence between dye molecules to get adsorbed on the surface. Among all the adsorbents, m-MNPs0.3-C/D0.5 has the highest adsorption capacity. Indeed, the qe values at an initial MB concentration of 400 mg L^{-1} were 285.31, 245.77, 381.74, 370.68 and 353.36 mg g^{-1} for MNPs0-C/D0.5 and its nanocomposites MNPs0.4-C/D0.5, m-MNPs0.3-C/D0.5, m-MNPs0.4-C/D0.5 and m-MNPs0.5-C/D0.5, respectively. This fact confirms the better retention of MB dye on m-MNPs-C/D0.5 adsorbents.

3.4.4. MB adsorption kinetics and isotherms modeling

Nonlinear forms of commonly used mathematical models; including Lagergren's pseudo-first-order and pseudo-second-order (PSO) kinetic equations were introduced to fit, the experimental data of MB adsorption (Equations (6) and (7)) and the results are showing in **Figure 8**.

The kinetic parameters were easily determined by fitting the experimental data in above equations (**Table 2**). The validity of the models was estimated using two statistical functions, namely the coefficient of determination (R^2, Equation (8)) and the sum square error (SSE, Equation (9)).[61]

$$R^2 = \frac{\left(q_{i,\ \text{meas}} - \overline{q}_{i,\ \text{cal}}\right)^2}{\sum_{i=1}^{n}\left(q_{i,\text{meas}} - \overline{q}_{i,\text{cal}}\right)^2 + \left(q_{i,\text{meas}} - q_{i,\text{cal}}\right)^2} \qquad (8)$$

$$\mathrm{SSE} = \sum_{i=1}^{n} \left(q_{i,\mathrm{exp}} - q_{i,\mathrm{cal}}\right)^2 \qquad (9)$$

where $q_{i,exp}$ and $q_{i,cal}$ are the adsorbed quantities of MB at experimental and theoretical equilibrium.

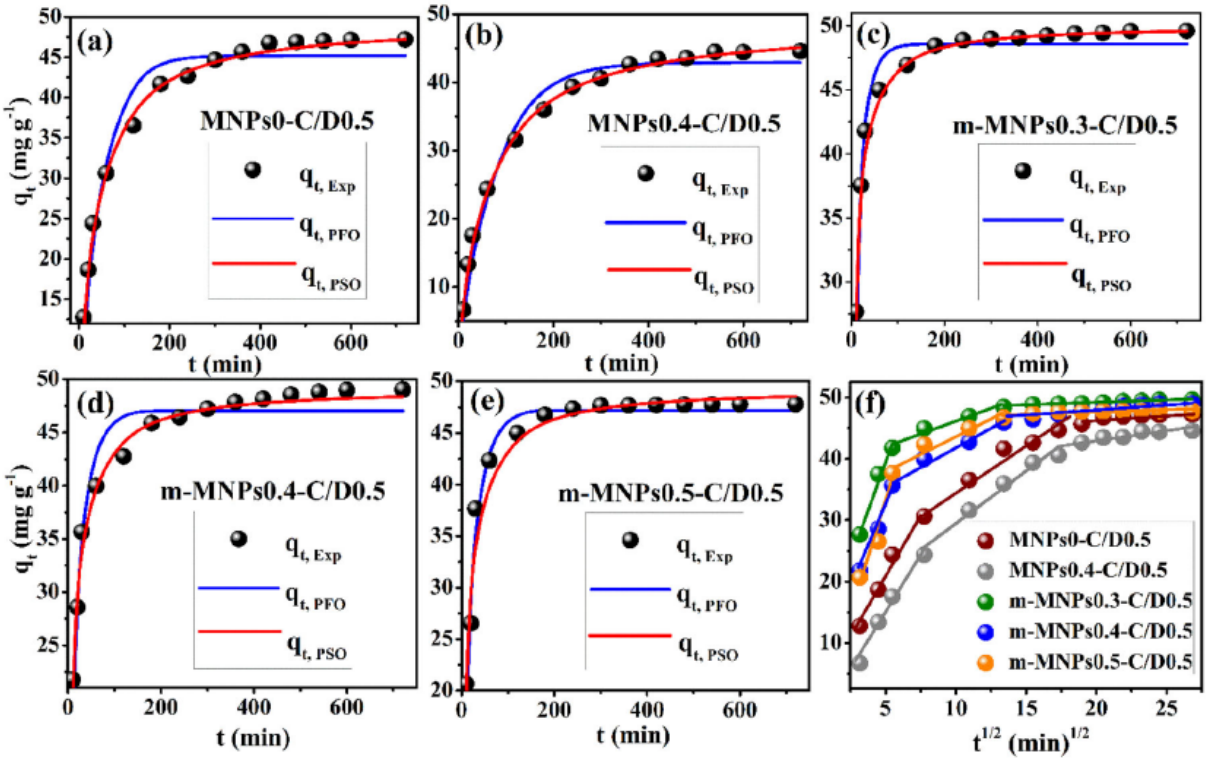

Figure 8. Adsorption kinetics modeling of MB dye on hydrogel matrix and its nanocomposites according to (a-e) nonlinear pseudo-first-order and pseudo-second-order models; (f) linear intra-particle diffusion kinetic model.

It can be clearly seen from **Table 2** that the PSO kinetic model is better adapted to describe the MB adsorption kinetics with R^2 values ≥ 0.995 and adsorption capacities calculated by this model (q_{e2}) that are very close to the experimental ones ($q_{e,exp}$). Further confirmation can be concluded from the low SSE values calculated for the PSO kinetic model. These findings suggest that the rate-limiting step is the electrostatic interactions developed between the adsorbent and adsorbate.[62] Similar results were previously reported for MB adsorption on Fe_3O_4/alginate/rice husk biocomposite and Magnetic chitosan hydrogel beads adsorbents.[20,57] Furthermore, the m-MNPs-C/D0.5 nanocomposite beads exhibit higher k_2 values compared to their MNPs0-C/D0.5 and MNPs0.4-C/D0.5 counterparts, highlighting the advantage of MNPs functionalization.

To better decipher the control mechanism of the adsorption process, the intra-particle diffusion model was evaluated. The adsorption rate kid is given by the following equation (Equation (10)).[63]

Table 2. Nonlinear kinetic and isotherm parameters of MB adsorption on the prepared hydrogel beads.

Kinetic models		Pseudo-first order model $q_t = q_{e1}(1 - e^{-k_1 t})$ (6)				Pseudo-second order model $q_t = \frac{k_2 q_{e2}^2 t}{[1+q_{e2}k_2 t]}$ (7)			
Adsorbent	$q_{e,exp}$ (mg g^{-1})	q_{e1} (mg g^{-1})	$k_1.10^2$ (min^{-1})	R^2	SSE	q_{e2} (mg g^{-1})	$k_2.10^2$	R^2	SSE
MNPs0-y	47.21	45.18	2.22	0.987	92.83	49.43	0.059	0.998	11.32
MNPs0.4-y	44.56	42.92	1.35	0.992	55.39	48.76	0.035	0.999	5.95
m-MNPs0.3-y	49.61	48.57	7.57	0.995	23.35	50.07	0.286	0.999	5.13
m-MNPs0.4-y	49.02	47.04	4.83	0.987	68.29	49.25	0.158	0.998	8.83
m-MNPs0.5-y	47.81	47.22	4.79	0.995	28.04	49.45	0.155	0.995	27.73

k_2 expressed in g mg^{-1}min^{-1}, $C_O = 50$ mg L^{-1}, adsorbent dose 1 g L^{-1}, at 25 °C, neutral pH.

Isotherm models		Freundlich model $q_e = K_F C_e^{1/n}$ (10)				Langmuir model $q_e = \frac{q_m K_L C_e}{[1+K_L C_e]}$ (11)				
Adsorbent[a]	$q_{e,exp}$ (mg g^{-1})	K_F (L g^{-1})	n (g L^{-1})	R^2	SSE	q_m (mg g^{-1})	K_L (L mg^{-1})	R^2	SSE	R_L[b]
MNPs0-y	380.91	83.97	4.32	0.969	16.56	380.96	0.04	0.992	5.72	0.507
MNPs0.4-y	330.97	63.45	4.01	0.956	16.71	331.82	0.03	0.991	3.93	0.563
m-MNPs0.3-y	529.35	151.89	5.02	0.927	84.87	529.26	0.13	0.999	0.70	0.229
m-MNPs0.4-y	498.75	139.45	4.93	0.926	75.75	502.98	0.11	0.999	1.40	0.268
m-MNPs0.5-y	479.02	121.69	4.67	0.945	50.33	476.93	0.08	0.998	2.28	0.342

[a] *$y = C/D0.5$.*

[b] *For $C0 = 25$ mg L^{-1}, the highest $C0$ lead to $R_L < 1$.*

$$q_t = k_{id} t^{1/2} + C \qquad (12)$$

where k_{id} is the rate constant (mg g^{-1} min$^{-1/2}$) and C is the intercept associated with the thickness of the boundary layer. These constants are deduced respectively from the slope and the y-intercept of the linear plot of (q_t) versus ($t^{1/2}$).

Figure 8(f) shows the linear plots of intra-particle diffusion model. The presence of multilinear plots for all adsorbents, which missed the original point, suggests that this model is not the only step controlling the absorption mechanism of MB and that this process is described by a succession of steps. Indeed, three distinguish successive stages were observed (**Table 2S**); (1) rapid external diffusion of MB to the beads surfaces ($k_{id\ I}$, ≤ 60 min), which was controlled by chemical adsorption (hydrogen bonding, van der Waals and electrostatic interactions); (2) slow internal diffusion ($k_{id\ II}$, 1h $\leq t \leq$ 5h), controlled by intraparticle diffusion as an adsorption rate-limiting step and (3) MB adsorption-desorption balance ($k_{id\ III}$, 5 h $\leq$ t $\leq$ 12 h). On the other hand, in the case of m-MNPs-C/D0.5 beads, almost all MB molecules ($C0 = 50$ mg L^{-1}) are adsorbed rapidly in the first step suggesting a high affinity of MB dye toward these materials, which leads to the highest ($k_{id\ I}$) values.

The equilibrium achieved between the MB molecules and the adsorbent surface can be described and quantified. For this purpose, two isotherm models were applied, namely Freundlich and Langmuir.[64,65] The Langmuir model assumes that the adsorption is localized and results only in the formation of a monolayer, whereas the Freundlich model is applicable in case of possible multilayer formation on the surface of the adsorbent with heterogeneous sites having different binding energies. The non-linear forms of these two models are listed in **Table 2**.

The favorability of adsorption process can also be expressed by the separation constant also designated by the dimensionless parameter (R_L) deduced from the Langmuir isotherm model.[31] It is expressed by the following equation (Equation (13)):

$$R_{\mathrm{L}} = \frac{1}{1 + K_{\mathrm{L}} C_0} \qquad (13)$$

According to the literature, adsorption is unfavorable when $R_L > 1$, linear ($R_L = 1$), favorable ($0 < R_L < 1$), or irreversible ($R_L = 0$).

Figure 9 illustrate the nonlinear fitting curves of the adsorption isotherms using the Freundlich and Langmuir models. The calculated parameters from these models and the SSE values are given in **Table 2**. The obtained results indicated the overall effectiveness of the Langmuir model for all the adsorbents, which show the highest R^2 (≥0.991) and the lowest SSE values compared to Freundlich's. These results reveal the homogeneity of the monolayer adsorption process at the surface of the adsorbents with no interactions between the adsorbed molecules on homogeneous sites. The R_L values were found to be lower than unite (R_L <1), which indicates favorable adsorption on all adsorbents. Furthermore, the feasibility of MB adsorption into nanocomposite beads was supported by Freundlich factor values (n) less than 10. Besides, the maximum equilibrium adsorption capacities (q_m) from Langmuir model are significantly higher for m-MNPs-C/D0.5 magnetic hydrogels than for the matrix. It must be mentioned that the optimum value of qm 529 mg g^{-1} was obtained for the m-MNPs0.3-C/D0.5 beads, which is increased by 149 mg g^{-1} compared to the matrix. An opposite result was obtained for MNPs0.4-C/D0.5.

3.4.5. Thermodynamic parameters and adsorption mechanism

The thermodynamic parameters, namely $\Delta G°$ (kJ mol^{-1}), $\Delta H°$ (kJ mol-1) and $\Delta S°$ (J mol^{-1}) are evaluated from the linear plot of ln K_d versus 1/T (**Figure 10(a)**) using the following equations (Equations (14)—(16)) and are summarized in **Table 3**.

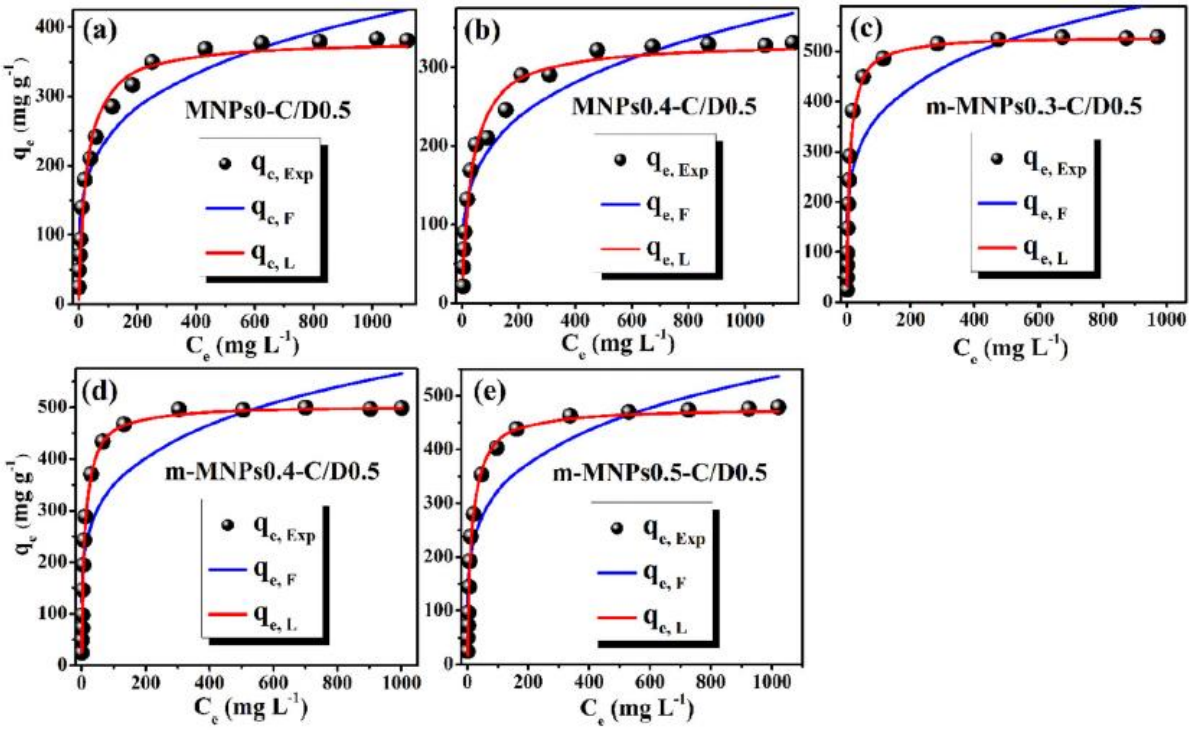

Figure 9. Isotherms nonlinear plots according to Freundlich (F) and Langmuir (L) models.

$$K_d = \frac{q_e}{C_e} \qquad (14)$$

$$\Delta G^0 = \Delta H^0 - T\Delta S^0 \qquad (15)$$

$$\mathrm{Ln}K_d = -\frac{\Delta H^0}{RT} + \frac{\Delta S^0}{R} \qquad (16)$$

where K_d is the equilibrium constant (L g^{-1}), T is the absolute temperature (K) and R is the universal gas constant (8.31 J $K^{-1}mol^{-1}$).

The negative values of $\Delta G°$ for all adsorbents indicate the spontaneity of the adsorption process within the experimental temperature range in this work. However, unlike the matrix, negative values of $\Delta H°$ of about 20 kJ mol^{-1} indicate the exothermic nature of MB physisorption through most likely hydrogen banding and electrostatic interactions.[26] While the negative $\Delta S°$ values reflect a decrease in magnitude mobility of the cationic molecules adsorbed on magnetic beads.

3.4.6. Regeneration study

To inspect the reusability of the magnetic adsorbents, the MNPs0.4-C/D0.5 and m-MNPs0.4-C/D0.5 beads as well as the MNPs0-C/D0.5 matrix was selected as regenerated adsorbents in five repeated adsorption/desorption cycles, as shown in **Figure 10(b)**. Both non-magnetic and magnetic nanocomposites are perfectly regenerated with desorption rates that exceed 94% and then reused without apparent loss of stability, reflecting the effectiveness of the selected regenerating agent as well as the mechanical robustness of examined beads. Compared to their starting state, the regenerated beads show an improvement in their removal efficiency after each adsorption/desorption cycle. This behavior is closely related to residual MB trapped within the beads that create more vacant spaces as observed previously for pure CMC and CMC/DS composite beads.[25,26]

Furthermore, this improvement is less evident for the nanocomposites than for the MNPs0-C/D0.5 matrix, which can be attributed to the less convoluted and narrow structure of the magnetic beads induced by MNPs and $m-MNP$s incorporation, making their desorption more difficult. It is worth noting that beyond cycle 5, unlike the magnetic beads, we observed the beginning of disintegration of the MNPs0-C/D0.5 pristine beads, which prevents the extensive use of this material for several adsorption/desorption cycles. This result highlights the advantage of using the nanofiller which improves the robustness of the beads.

To evaluate the maximum adsorption capacity of regenerated magnetic beads, isotherms were performed on beads from the third cycle. The obtained results as well as their modeling with the linearized equations of Langmuir and Freundlich are shown in **Figure 1S** (see supplementary data). As revealed, MB adsorption on all adsorbents was perfectly described by the Langmuir model as $R^2 >$ 0.999 (**Table 3S**). On the other hand, the beneficial impact of regeneration was attested through the elevated qm values of the regenerated beads as compared to the starting ones. Indeed, the qm values

of the regenerated beads R-MNPs0-C/D0.5, R-MNPs0.4-C/D0.5 and R-m-MNPs0.4C/D0.5 was respectively 584.7, 386.1 and 595.2 mg g^{-1}, which exceed those of the starting counterpart by about 200, 49 and 90 mg g^{-1}, respectively.

The proposed MB adsorption mechanism on magnetic hydrogels hydrogel is shown in **Figure 10C**. Similar to that of the MNPs0-C/D0.5 matrix,[26] the active groups -COO^-/-O-SO_3^-/-OH available on the surface of the CMC/DS adsorbent system are the focal points which contribute to the dye molecules binding through electrostatic interactions and hydrogen bonding.

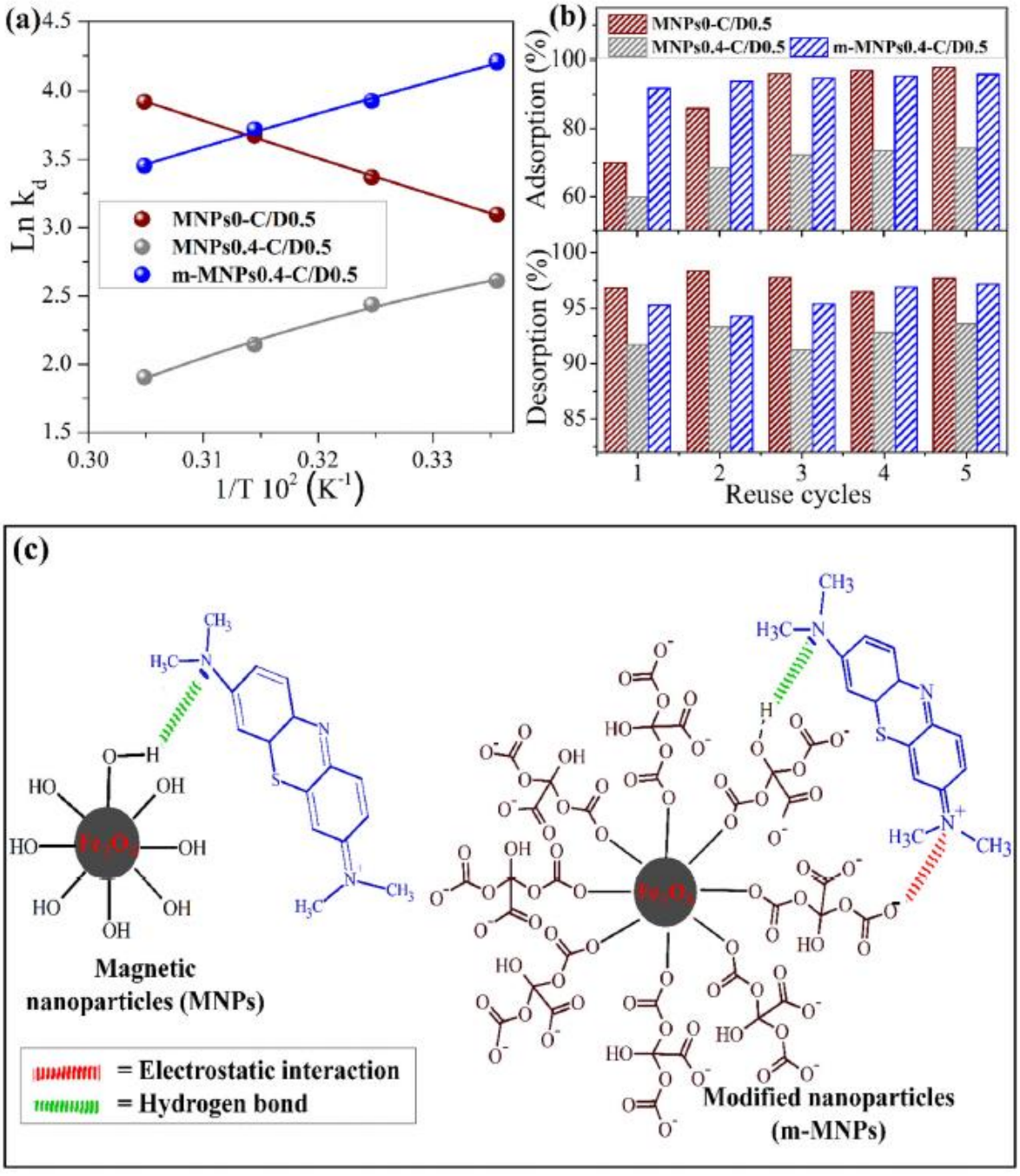

Figure 10. (a) Linear fitting plots of experimental thermal adsorption data; (b) Adsorbents regeneration assays for five cycles; (c) Proposed mechanism for MB adsorption onto unmodified magnetite nanoparticles ($MNPs$) and functionalized ones ($m-MNPs$).

Table 3. Thermodynamic parameters of MB adsorption on matrix beads and its nanocomposites.

Adsorbent	C_0 (mg L^{-1})	ΔG^0 (kJ mol^{-1})				ΔH^0 (kJ mol^{-1})	ΔS^0 (J mol^{-1} K^{-1})
		298	308	318	328		
MNPs0-y	200	−7.671	−8.627	−9.717	−10.699	22.647	101.680
MNPs0.4-y	200	−6.468	−6.036	−5.309	−5.318	−19.907	−43.839
m-MNPs0.4-y	200	−10.433	−9.733	−9.222	−9.419	−20.122	−32.533

y = C/D0.5.

In addition, in the presence of pure magnetite MNPs, additional hydrogen bonding may occur between their surface hydroxyls and the amine and/or imine groups ($-RCH = NR$) of MB dye. Similarly, the carboxylate and hydroxyl groups of citrate ions in the surface of m-MNPs might also be involved in the stabilization of the dye-nanocomposite complex. To investigate the contribution of the cation exchange process in MB removal, we analyzed by $ICP-MS$ the solutions recovered after MB adsorption.

Table 4. Langmuir adsorption capacities (q_m) of MB dye on the hydrogel beads prepared in this study and those found in the literature.

Adsorbant	q_m (mg g^{-1})	References
Magnetic alginate/clinoptilolite/Fe_3O_4 composite	12	[66]
Carboxymethyl cellulose coated Fe_3O_4 at SiO_2 core-shell magnetic nanoparticles	22	[67]
Montmorillonite nanosheets/chitosan hydrogels	530	[68]
Lignin-derived magnetic activated carbons	220	[69]
Magnetic/activated charcoal/βCyclodextrin/alginate polymer nanocomposite	10	[70]
Magnetic chitosan hydrogel beads	251	[20]
Magnetic alginate/rice husk bio-composite	274	[57]
Nanocomposite beads prepared by unmodified magnetic nanoparticles MNPs0.4-C/D0.5	331	Values obtained in this study
Nanocomposite beads prepared by modified magnetic nanoparticles m-MNPsx-C/D0.5	476–529	
Regenerated magnetic beads, R-MNPs0.4-C/D0.5	386	
Regenerated magnetic beads, R-m-MNPs0.4-C/D0.5	595	

The aim of this analysis was to determine the quantity of $Al^{3+}/Fe^{3+}/Fe^{2+}$ ions (from the cross-linking agent and the MNPs) exchanged with the MB dye molecules and to investigate the mechanical stability of these beads during use. **Table 4S** summarizes the quantities of ions initially present in the beads and those released during the experiment. As observed, the amount of ions released from the beads was extremely low compared to that within the beads (<3%) indicating that the contribution of the cation exchange process in MB removal is minor and only a small fraction of MB molecules are retained via this process. It should be noted that the concentration of released ions was insignificant to be considered as secondary pollution. Furthermore, this result confirms the mechanical stability of the beads in the investigated conditions while keeping their spherical shape after use.

The stability of the nanocomposite beads after MB adsorption was also investigated using XRD. The comparison of the XRD data before and after the MB dye adsorption process (**Figure 2S**) showed that there were some changes in peak position and intensities as well as the disappearance of some peaks as observed around $2\theta = 21.36°$ and 53.5°, which may be a marker of MB dye adsorption. Based on these results it can be concluded that the crystallinity of nanocomposite beads was not significantly affected confirming their crystalline stabilities.

3.4.7. Comparative study of alternative adsorbents

For further evaluation of MB dye adsorption efficiency on our hydrogel beads, a comparison of their qm capacities with those of previous similar studies was provided in **Table 4**. It is evident that our materials are not only promising adsorbents as they have higher qm values than certain previous studies, but also show significantly improved adsorption performance after regeneration and reuse for five adsorption/-desorption cycles. Beside, our nanocomposite adsorbents combine the highest adsorption capacities with good magnetic separation properties and thus can be considered as attractive and low-cost adsorbents for an efficient recovery of cationic dyes from contaminated water. However, their use is not recommended for strongly acidic or basic environments leading to their disintegration as was observed in the swelling study.

4. Conclusions

In this study, magnetics nanocomposite beads enclosing Fe_3O_4 nanoparticles initially synthesized and functionalized with citrate ions were successfully elaborated by the ecofriendly ionotropic gelation method, characterized, and then evaluated as promising helpful devices for MB removal from contaminated water. The results showed a rather rough and compact external surface with a well-defined interconnected microporous structure for the m-MNPs-C/D0.5 magnetic hydrogels compared to the pristine matrix. Besides, swelling and adsorption performances were significantly improved following the incorporation of $m-MNP$s while an opposite effect was observed by introducing MNPs nanoparticles. MB removal study results revealed that unlike the blank beads, the adsorption process on their magnetic counterparts was exothermic in nature and a very good agreement between the experimental results and those of the PSO kinetic and Langmuir models was observed. Such results confirm the monolayer adsorption of MB via mainly physical interactions of hydrogen bonding and electrostatic interactions established between the carboxylate, sulfate and hydoxyl functional groups ($-COO^-$, $-O-SO_3^-$ and -OH) at adsorbents surface and those of the cationic dye. Furthermore, the removal efficiency of the beads studied for five adsorption-desorption cycles is increased after each regeneration cycle, reaching an equilibrium at the third cycle. To sum up, the hydrogel beads developed in the current study could potentially be used for MB removal by combining the magnetic properties suitable for easy separation with good handling properties offered by the polymer beads.

References

[1] Abedin, M. A.; Collins, A. E.; Habiba, U.; Shaw, R. Climate [17] Change, Water Scarcity, and Health Adaptation in Southwestern Coastal Bangladesh. Int. J. Disaster Risk Sci. **2019**, 10, 28-42. DOI: **10.1007/s13753-018-0211-8**.

[2] Legorreta-Castaneda, A. J.; Lucho-Constantino, C. A.; Beltran-Hernandez, R. I.; Coronel-Olivares, C.; Vazquez-Rodriguez, G. A. Biosorption of Water Pollutants by Fungal Pellets. Water (Switzerland) **2020**, 12, 1155. DOI: **10.3390/w12041155**.

[3] Bala, S.; Garg, D.; Thirumalesh, B. V.; Sharma, M.; Sridhar, K.; Inbaraj, B. S.; Tripathi, M. Recent Strategies for Bioremediation of Emerging Pollutants: A Review for a Green and Sustainable Environment. Toxics **2022**, 10, 484. DOI: **10.3390/toxics 10080484**.

[4] Kaur, N.; Brraich, O. S. Impact of Industrial Effluents on Physico-Chemical Parameters of Water and Fatty Acid Profile of Fish, Labeo rohita (Hamilton), Collected from the Ramsar Sites of

Punjab, India. Environ. Sci. Pollut. Res. Int. **2022**, 29, 11534-11552. DOI: **10.1007/S11356-021-16429-2/FIGURES/6**.

[5] Hernandez-Montoya, V.; Perez-Cruz, M. A.; Mendoza-Castillo, D. I.; Moreno-Virgen, M. R.; Bonilla-Petriciolet, A. Competitive Adsorption of Dyes and Heavy Metals on Zeolitic Structures. J. Environ. Manage. **2013**, 116, 213-221. DOI: **10.1016/j.jenvman. 2012.12.010**.

[6] Berradi, M.; Hsissou, R.; Khudhair, M.; Assouag, M.; Cherkaoui, O.; El Bachiri, A.; El Harfi, A. Textile Finishing Dyes and Their Impact on Aquatic Environs. Heliyon **2019**, 5, e02711. DOI: **10.1016/j.heliyon.2019.e02711**.

[7] Chingrishon, K.; Geeta, S. A Review of Various Treatment Methods for the Removal of Dyes from Textile Effluent. Recent Prog. Mater. **2022**, 4, 1-15. DOI: **10.21926/RPM.2204028**.

[8] Katheresan, V.; Kansedo, J.; Lau, S. Y. Efficiency of Various Recent Wastewater Dye Removal Methods: A Review. J. Environ. Chem. Eng. **2018**, 6, 4676-4697. DOI: **10.1016/j.jece. 2018.06.060**.

[9] De Gisi, S.; Lofrano, G.; Grassi, M.; Notarnicola, M. Characteristics and Adsorption Capacities of Low-Cost Sorbents for Wastewater Treatment: A Review. Sustain. Mater. Technol. **2016**, 9, 10-40. DOI: **10.1016/j.susmat.2016.06.002**.

[10] Ngulube, T.; Gumbo, J. R.; Masindi, V.; Maity, A. An Update on Synthetic Dyes Adsorption onto Clay Based Minerals: A State-of-Art Review. J. Environ. Manage. **2017**, 191, 35-57. DOI: **10.1016/j.jenvman.2016.12.031**.

[11] Djilani, C.; Zaghdoudi, R.; Djazi, F.; Bouchekima, B.; Lallam, A.; Modarressi, A.; Rogalski, M. Adsorption of Dyes on Activated Carbon Prepared from Apricot Stones and Commercial Activated Carbon. J. Taiwan Inst. Chem. Eng. **2015**, 53, 112-121. DOI: **10.1016/j.jtice.2015.02.025**.

[12] Qi, X.; Wu, L.; Su, T.; Zhang, J.; Dong, W. Polysaccharide-Based Cationic Hydrogels for Dye Adsorption. Colloids Surf. B Biointerfaces. **2018**, 170, 364-372. DOI: **10.1016/j.colsurfb.2018.06.036**.

[13] Lehocký, M.; Mracek, A. Improvement of Dye Adsorption on Synthetic Polyester Fibers by Low Temperature Plasma PreTreatment. Czechoslov. J. Phys. **2006**, 56, 1277-1282. DOI: **10. 1007/s10582-006-0362-5**.

[14] Amode, J. O.; Santos, J. H.; Md. Alam, Z.; Mirza, A. H.; Mei, C. C. Adsorption of Methylene Blue from Aqueous Solution Using Untreated and Treated (Metroxylon spp.) Waste Adsorbent: Equilibrium and Kinetics Studies. Int. J. Ind. Chem. **2016**, 7, 333-345. DOI: **10.1007/s40090-016-0085-9**.

[15] Mokadem, Z.; Mekki, S.; Saidi-Besbes, S.; Agusti, G.; Elaissari, A.; Derdour, A. Triazole Containing Magnetic Core-Silica Shell Nanoparticles for Pb2+, Cu2+ and Zn2+ Removal. Arab. J. Chem. **2017**, 10, 1039-1051. DOI: **10.1016/j.arabjc.2016.12.008**.

[16] Kumar Gupta, V.; Agarwal, S.; Asif, M.; Fakhri, A.; Sadeghi, N. Application of Response Surface Methodology to Optimize the Adsorption Performance of a Magnetic Graphene Oxide Nanocomposite Adsorbent for Removal of Methadone from the Environment. J. Colloid Interface Sci. **2017**, 497, 193-200. DOI: **10.1016/j.jcis.2017.03.006**.

[17] Xia, Y.; Yao, Q.; Zhang, W.; Zhang, Y.; Zhao, M. Comparative Adsorption of Methylene Blue by Magnetic Baker's Yeast and EDTAD-Modified Magnetic Baker's Yeast: Equilibrium and Kinetic Study. Arab. J. Chem. **2019**, 12, 2448-2456. DOI: **10. 1016/j.arabjc.2015.03.010**.

[18] Salehi, E.; Madaeni, S. S.; Rajabi, L.; Vatanpour, V.; Derakhshan, A. A.; Zinadini, S.; Ghorabi, S.; Ahmadi Monfared, H. Novel Chitosan/Poly(Vinyl) Alcohol Thin Adsorptive Membranes Modified with Amino Functionalized Multi-Walled Carbon Nanotubes for Cu(II) Removal from Water: Preparation, Characterization, Adsorption Kinetics and Thermodynamics. Sep. Purif. Technol. **2012**, 89, 309-319. DOI: **10.1016/j.seppur.2012.02.002**.

[19] Nicola, R.; Costisor, O.; Ciopec, M.; Negrea, A.; Lazau, R.; Ianasi, C.; Piciorus, E.-M.; Len, A.; Almasy, L.; Szerb, E. I.; et al. Silica-Coated Magnetic Nanocomposites for Pb2+ Removal from Aqueous Solution. Appl. Sci. **2020**, 10, 2726. DOI: **10.3390/app10082726**.

[20] Jamali, M.; Akbari, A. Facile Fabrication of Magnetic Chitosan Hydrogel Beads and Modified by Interfacial Polymerization Method and Study of Adsorption of Cationic/Anionic Dyes from Aqueous Solution. J. Environ. Chem. Eng. **2021**, 9, 105175. DOI: **10.1016/j.jece.2021.105175**.

[21] Liu, L.; Chang, S.; Wang, Y.; Zhao, H.; Wang, S.; Zheng, C.; Ding, Y.; Ren, S.; Zhang, J.; Guo, Y.-R.; et al. Facile Fabrication of Ion-Imprinted Fe_3O_4/Carboxymethyl Cellulose Magnetic Biosorbent: Removal and Recovery Properties for Trivalent La Ions. RSC Adv. **2021**, 11, 25258-25265. DOI: 10.1039/ D1RA03647E.

[22] Xu, Y.; Ma, X. Y.; Gong, W.; Li, X.; Huang, H. B.; Zhu, X. M. Nanoparticles Based on Carboxymethylcellulose-Modified Rice Protein for Efficient Delivery of Lutein. Food Funct. **2020**, 11 , 2380-2394. DOI: **10.1039/c9fo02439e**.

[23] Nuisin, R.; Siripongpreda, T.; Watcharamul, S.; Siralertmukul, K.; Kiatkamjornwong, S. Facile Syntheses of Physically Crosslinked Carboxymethyl Cellulose Hydrogels and Nanocomposite Hydrogels for Enhancing Water Absorbency and Adsorption of Sappan Wood Dye. ChemistrySelect **2022**, 7, 4598. DOI: **10.1002/slct.202104598**.

[24] Ure, D.; Mutus, B. The Removal of Inorganic Phosphate from Water Using Carboxymethyl Cellulose-Iron Hydrogel Beads. J. Chem. Technol. Biotechnol. **2021**, 96, 38-47. DOI: **10.1002/jctb. 6544**.

[25] Benhalima, T.; Ferfera-Harrar, H.; Lerari, D. Optimization of Carboxymethyl Cellulose Hydrogels Beads Generated by an Anionic Surfactant Micelle Templating for Cationic Dye Uptake: Swelling, Sorption and Reusability Studies. Int. J. Biol. Macromol. **2017**, 105, 1025-1042. DOI: **10.1016/j.ijbiomac.2017. 07.135**.

[26] Benhalima, T.; Ferfera-Harrar, H. Eco-Friendly Porous Carboxymethyl Cellulose/Dextran Sulfate Composite Beads as Reusable and Efficient Adsorbents of Cationic Dye Methylene Blue. Int. J. Biol. Macromol. **2019**, 132, 126-141. DOI: **10.1016/ j.ijbiomac.2019.03.164**.

[27] Ba-Abbad, M. M.; Benamour, A.; Ewis, D.; Mohammad, A. W.; Mahmoudi, E. Synthesis of Fe_3O_4 Nanoparticles with Different Shapes through a Co-Precipitation Method and Their Application. JOM. **2022**, 74, 3531-3539. DOI: **10.1007/S11837-022-05380-3/TABLES/1**.

[28] Idris, A.; Ismail, N. S. M.; Hassan, N.; Misran, E.; Ngomsik, A.-F. Synthesis of Magnetic Alginate Beads Based on Maghemite Nanoparticles for Pb(II) Removal in Aqueous Solution. J. Ind. Eng. Chem. **2012**, 18, 1582-1589. DOI: **10.1016/j.jiec.2012.02. 018**.

[29] Shi, X. N.; Wang, W. B.; Wang, A. Q. Effect of Surfactant on Porosity and Swelling Behaviors of Guar Gum-g-Poly(Sodium Acrylate-co-Styrene)/Attapulgite Superabsorbent Hydrogels. Colloids Surf. B Biointerfaces. **2011**, 88, 279-286. DOI: **10.1016/ j.colsurfb.2011.07.002**.

[30] Čerović, L. S.; Milonjic, S. K.; Todorovic, M. B.; Trtanj, M. I.; Pogozhev, Y. S.; Blagoveschenskii, Y.; Levashov, E. A. Point of Zero Charge of Different Carbides. Colloids Surf. A Physicochem. Eng. Asp. **2007**, 297, 1-6. DOI: **10.1016/j.colsurfa. 2006.10.012**.

[31] Ferfera-Harrar, H.; Benhalima, T.; Lerari, D. Sustainable Hydrogel Nanocomposites Based on Grafted Chitosan and Clay for Effective Adsorption of Cationic Dye. Int. J. Mater. Metall. Eng. **2020**, 14, 5-15. DOI: **10.5281/ZENODO.3607898**.

[32] Davodi, B.; Jahangiri, M.; Ghorbani, M. Magnetic Fe_3O_4 @ Polydopamine Biopolymer: Synthesis, Characterization and Fabrication of Promising Nanocomposite. J. Vinyl Addit. Technol. **2019**, 25, 41-47. DOI: **10.1002/vnl.21627**.

[33] Zhang, Y.; Xu, J.; Li, Q.; Cao, D.; Li, S. The Effect of the Particle Size and Magnetic Moment of the Fe_3O_4 Superparamagnetic Beads on the Sensitivity of Biodetection. AIP Adv. **2019**, 9, 015215. DOI: **10.1063/1.5050034**.

[34] Rodriguez, A. F. R.; Rocha, C. O.; Piazza, R. D.; Dos Santos, C. C.; Morales, M. A.; Faria, F. S. E. D. V.; Iqbal, M. Z.; Barbosa, L.; Chaves, Y. O.; Mariuba, L. A.; et al. Synthesis, Characterization and Applications of Maghemite Beads Functionalized with Rabbit Antibodies. Nanotechnology. **2018**, 29, 365701. DOI: **10.1088/1361-6528/aacc21**.

[35] Chong, W. H.; Ng, Q. H.; Lim, J. K.; Yeap, S. P.; Low, S. C. Study on the Enhancement of Colloidal Stable Poly(Sodium 4-Styrene Sulfonate) Coated Magnetite Nanoparticles and Regeneration Capability for Rapid Magnetophoretic Removal of Organic Dye. J. Chem. Technol. Biotechnol. **2020**, 95, 30933104. DOI: **10.1002/jctb.6485**.

[36] Dawn, R.; Zzaman, M.; Faizal, F.; Kiran, C.; Kumari, A.; Shahid, R.; Panatarani, C.; Joni, I. M.; Verma, V. K.; Sahoo, S. K.; et al. Origin of Magnetization in Silica-Coated Fe3O4 Nanoparticles Revealed by Soft X-Ray Magnetic Circular Dichroism. Braz. J. Phys. **2022**, 52, 1-12. DOI: **10.1007/S13538-022-01102-X/FIGURES/7**.

[37] Xu, B.; Zheng, C.; Zheng, H.; Wang, Y.; Zhao, C.; Zhao, C.; Zhang, S. Polymer-Grafted Magnetic Microspheres for Enhanced Removal of Methylene Blue from Aqueous Solutions. RSCAdv. **2017**, 7, 47029-47037. DOI: **10.1039/C7RA06810G**.

[38] Hu, H.; Yang, L.; Lin, Z.; Xiang, X.; Jiang, X.; Hou, L. Preparation and Characterization of Novel Magnetic Fe3O4/Chitosan/Al(OH)3 Beads and Its Adsorption for Fluoride. Int. J. Biol. Macromol. **2018**, 114, 256-262. DOI: **10. 1016/j.ijbiomac.2018.03.094**.

[39] Pan, X.; Zuo, G.; Su, T.; Cheng, S.; Gu, Y.; Qi, X.; Dong, W. Polycarboxylic Magnetic Polydopamine Sub-Microspheres for Effective Adsorption of Malachite Green. Colloids Surf. A Physicochem. Eng. Asp. **2019**, 560, 106-113. DOI: **10.1016/j.col-surfa.2018.10.014**.

[40] Verma, R.; Asthana, A.; Singh, A. K.; Prasad, S.; Susan, M. A. B. H. Novel Glycine-Functionalized Magnetic Nanoparticles Entrapped Calcium Alginate Beads for Effective Removal of Lead. Microchem. J. **2017**, 130, 168-178. DOI: **10.1016/j.microc. 2016.08.006**.

[41] Tang, X.; Tang, P.; Liu, L. Preparation of Tetraethylenepentamine Modified Magnetic Graphene Oxide for Adsorption of Dyes from Aqueous Solution. J. Braz. Chem. Soc. **2017**, 29, 334-342. DOI: **10.21577/0103-5053.20170145**.

[42] Fatima, H.; Lee, D. W.; Yun, H. J.; Kim, K. S. Shape-Controlled Synthesis of Magnetic Fe3O4 Nanoparticles with Different Iron Precursors and Capping Agents. RSC Adv. **2018**, 8, 2291722923. DOI: **10.1039/c8ra02909a**.

[43] Jameel Abdulghani, A.; Madhloom Al-Ogedy, W. Synthesis and Characterization of Multishapes of Fe3O4 Nanoparticle by Solve-Hydrothermal Method Using Microwave Radiation. Baghdad Sci. J. **2016**, 13, 0331. DOI: **10.21123/bsj.2016.13.2. 0331**.

[44] Zhao, S.; Lee, D. G.; Kim, C. W.; et al. Synthesis of Magnetic Nanoparticles of Fe_3O_4 and $CoFe_2O_4$ and Their Surface Modification by Surfactant Adsorption. Bull. Korean Chem. Soc. **2006**, 27, 237-242. DOI: **10.5012/bkcs.2006.27.2.237**.

[45] Na, Y.; Yang, S.; Lee, S. Evaluation of Citrate-Coated Magnetic Nanoparticles as Draw Solute for Forward Osmosis. Desalination. **2014**, 347, 34-42. DOI: **10.1016/j.desal.2014.04. 032**.

[46] Konwar, A.; Gogoi, A.; Chowdhury, D. Magnetic alginate-Fe3O4 Hydrogel Fiber Capable of Ciprofloxacin Hydrochloride Adsorption/Separation in Aqueous Solution. RSC Adv. **2015**, 5, 81573-81582. DOI: **10.1039/C5RA16404D**.

[47] Ismail, R. A.; Sulaiman, G. M.; Abdulrahman, S. A.; Marzoog, T. R. Antibacterial Activity of Magnetic Iron Oxide Nanoparticles Synthesized by Laser Ablation in Liquid. Mater. Sci. Eng. C Mater. Biol. Appl. **2015**, 53, 286-297. DOI: **10.1016/ j.msec.2015.04.047**.

[48] Thottoli, A. K.; Unni, A. K. A. Effect of Trisodium Citrate Concentration on the Particle Growth of ZnS Nanoparticles. J. Nanostruct. Chem. **2013**, 3, 56. DOI: **10.1186/2193-8865-3-56**.

[49] Bardajee, G. R.; Hooshyar, Z. A Novel Biocompatible Magnetic Iron Oxide Nanoparticles/Hydrogel Based on Poly(Acrylic Acid) Grafted onto Starch for Controlled Drug Release. J. Polym. Res. **2013**, 20, 298. DOI: **10.1007/s10965-013-0298-y**.

[50] Schott, H. Swelling Kinetics of Polymers. J. Macromol. Sci. Part B. **1992**, 31, 1-9. DOI: **10.1080/00222349208215453**.

[51] Ganji, F.; Vasheghani-Farahani, S.; Vasheghani-Farahani, E. Theoretical Description of Hydrogel Swelling: A Review. Iran. Polym. J **2010**, 19, 375-398.

[52] Durmaz, S.; Okay, O. Acrylamide/2-Acrylamido-2-Methylpropane Sulfonic Acid Sodium Salt-Based Hydrogels: Synthesis and Characterization. Polymer (Guildf). **2000**, 41, 3693-3704. DOI: **10.1016/S0032-3861(99)00558-3**.

[53] Ferfera-Harrar, H.; Benhalima, T.; Sadi, A. Development of Functional Chitosan-Based Superabsorbent Hydrogel Nanocomposites for Adsorptive Removal of Basic Red 46 Textile Dye. Polym. Bull. **2022**, 79, 6141-6172. DOI: **10.1007/ s00289-021-03795-7**.

[54] Ferfera-Harrar, H.; Aouaz, N.; Dairi, N. Environmental-Sensitive Chitosan-g-Polyacrylamide/Carboxymethylcellulose Superabsorbent Composites for Wastewater Purification I: Synthesis and Properties. Polym. Bull. **2016**, 73, 815-840. DOI: **10.1007/s00289-015-1521-2**.

[55] Nguyen, H. T.; Ngwabebhoh, F. A.; Saha, N.; Saha, T.; Saha, P. Gellan Gum/Bacterial Cellulose Hydrogel Crosslinked with Citric Acid as an Eco-Friendly Green Adsorbent for Safranin and Crystal Violet Dye Removal. Int. J. Biol. Macromol. **2022**, 222, 77-89. DOI: **10.1016/J.IJBIOMAC.2022.09.040**.

[56] Maponya, T.; Ramohlola, K.; Kera, N.; Modibane, K.; Maity, A.; Katata-Seru, L.; Hato, M. Influence of Magnetic Nanoparticles on Modified Polypyrrole/m-Phenylediamine for Adsorption of Cr(VI) from Aqueous Solution. Polymers (Basel). **2020**, 12, 679. DOI: **10.3390/polym12030679**.

[57] Alver, E.; Metin, A. U.; Brouers, F. Methylene Blue Adsorption on Magnetic Alginate/Rice Husk Bio-Composite. Int. J. Biol. Macromol. **2020**, 154, 104-113. DOI: **10.1016/J.IJBIOMAC.2020.02.330**.

[58] Mahdavinia, G. R.; Iravani, S.; Zoroufi, S.; Hosseinzadeh, H. Magnetic and K^+-Cross-Linked Kappa-Carrageenan Nanocomposite Beads and Adsorption of Crystal Violet. Iran. Polym. J. **2014**, 23, 335-344. DOI: **10.1007/s13726-014-0229-8**.

[59] Zheng, M.; Cai, K.; Chen, M.; Zhu, Y.; Zhang, L.; Zheng, B. pH-Responsive Poly(Gellan Gum-co-Acrylamide-co-Acrylic Acid) Hydrogel: Synthesis, and Its Application for Organic Dye Removal. Int. J. Biol. Macromol. **2020**, 153, 573-582. DOI: **10. 1016/J.IJBIOMAC.2020.03.024**.

[60] Han, S.; Wang, T.; Li, B. Preparation of a Hydroxyethyl-Titanium Dioxide-Carboxymethyl Cellulose Hydrogel Cage and Its Effect on the Removal of Methylene Blue. J. Appl. Polym. Sci. **2017**, 134, 44925. DOI: **10.1002/app.44925**.

[61] Zamouche, M.; Habib, A.; Saaidia, K.; Bencheikh Lehocine, M. Batch Mode for Adsorption of Crystal Violet by Cedar Cone Forest Waste. SN Appl. Sci. **2020**, 2, 198. DOI: **10.1007/s42452-020-1976-0**.

[62] Zhen, Y.; Ning, Z.; Shaopeng, Z.; Yayi, D.; Xuntong, Z.; Jiachun, S.; Weiben, Y.; Yuping, W.; Jianqiang, C. A pH- and Temperature-Responsive Magnetic Composite Adsorbent for Targeted Removal of Nonylphenol. ACS Appl. Mater. Interfaces. **2015**, 7, 24446-24457. DOI: **10.1021/acsami.5b08709**.

[63] Doke, K. M.; Khan, E. M. Equilibrium, Kinetic and Diffusion Mechanism of Cr(VI) Adsorption onto Activated Carbon Derived from Wood Apple Shell. Arab. J. Chem **2017**, 10, S252-S260. DOI: **10.1016/j.arabjc.2012.07.031**.

[64] Freundlich, H. Uber Die Adsorption in Losungen. Z. Phys. Chem. **1907**, 57U, 385-470. DOI: **10.1515/zpch-1907-5723**.

[65] Langmuir, I. The Adsorption of Gases on Plane Surfaces of Glass, Mica and Platinum. J. Am. Chem. Soc. **1918**, 40, 13611403. DOI: **10.1021/ja02242a004**.

[66] Noori, M.; Tahmasebpoor, M.; Foroutan, R. Enhanced Adsorption Capacity of Low-Cost Magnetic Clinoptilolite Powders/Beads for the Effective Removal of Methylene Blue: Adsorption and Desorption Studies. Mater. Chem. Phys. **2022**, 278, 125655. DOI: **10.1016/j.matchemphys.2021.125655**.

[67] Zirak, M.; Abdollahiyan, A.; Eftekhari-Sis, B.; Saraei, M. Carboxymethyl Cellulose Coated Fe_3O_4@SiO_2 Core-Shell Magnetic Nanoparticles for Methylene Blue Removal: Equilibrium,

Kinetic, and Thermodynamic Studies. Cellulose. **2018**, 25, 503-515. DOI: **10.1007/s10570-017-1590-5**.

[68] Kang, S.; Zhao, Y.; Wang, W.; Zhang, T.; Chen, T.; Yi, H.; Rao, F.; Song, S. Removal of Methylene Blue from Water with Montmorillonite Nanosheets/Chitosan Hydrogels as Adsorbent. Appl. Surf. Sci. **2018**, 448, 203-211. DOI: **10.1016/j.apsusc.2018. 04.037**.

[69] Yu, L.; Keffer, D. J.; Hsieh, C.-T.; Scroggins, J. R.; Chen, H.; Dai, S.; Harper, D. P. Lignin-Derived Magnetic Activated Carbons for Effective Methylene Blue Removal. Ind. Eng. Chem. Res. **2022**, 61, 11840-11850. DOI: **10.1021/acs.iecr.2c02311**.

[70] Yadav, S.; Asthana, A.; Chakraborty, R.; Jain, B.; Singh, A. K.; Carabineiro, S. A. C.; Susan, M. A. B. H. Cationic Dye Removal Using Novel Magnetic/Activated Charcoal/b-Cyclodextrin/ Alginate Polymer Nanocomposite. Nanomaterials. **2020**, 10, 170. DOI: **10.3390/nano10010170**.